Systematic study of probable projectile-target combinations for the synthesis of the superheavy nucleus $^{302}120$

K. P. Santhosh* and V. Safoora

School of Pure and Applied Physics, Swami Anandatheertha Campus, Kannur University, Payyanur 670327, Kerala, India

(Received 22 March 2016; revised manuscript received 5 July 2016; published 31 August 2016)

Probable projectile-target combinations for the synthesis of the superheavy element $^{302}120$ have been studied taking the Coulomb and proximity potential as the interaction barrier. The probabilities of the compound nucleus formation P_{CN} for the projectile-target combinations found in the cold reaction valley of $^{302}120$ are estimated. At energies near and above the Coulomb barrier, we have calculated the capture, fusion, and evaporation residue cross sections for the reactions of all probable projectile-target combinations so as to predict the most promising projectile-target combinations for the synthesis of the superheavy element $^{302}120$ in heavy-ion fusion reactions. The calculated fusion and evaporation cross sections for the more asymmetric ("hotter") projectile-target combination is found to be higher than the less asymmetric ("colder") combination. It can be seen from the nature of the quasifission barrier height, mass asymmetry, the probability of compound nucleus formation, survival probability, and excitation energy, the systems $^{44}Ar + ^{258}No$, $^{46}Ar + ^{256}No$, $^{48}Ca + ^{254}Fm$, $^{50}Ca + ^{252}Fm$, $^{54}Ti + ^{248}Cf$, and $^{58}Cr + ^{244}Cm$ in deep region I of the cold reaction valley and the systems $^{62}Fe + ^{240}Pu$, $^{64}Fe + ^{238}Pu$, $^{68}Ni + ^{234}U$, $^{70}Ni + ^{232}U$, $^{72}Ni + ^{230}U$, and $^{74}Zn + ^{228}Th$ in the other cold valleys are identified as the better projectile-target combinations for the synthesis of $^{302}120$. Our predictions on the synthesis of $^{302}120$ superheavy nuclei using the combinations $^{54}Cr + ^{248}Cm$, $^{58}Fe + ^{244}Pu$, $^{64}Ni + ^{238}U$, and $^{50}Ti + ^{249}Cf$ are compared with available experimental data and other theoretical predictions.

DOI: 10.1103/PhysRevC.94.024623

I. INTRODUCTION

Heavy-ion fusion reactions have been widely used to synthesize elements in the heavy and superheavy (SH) regions, and now nuclear reactions induced by heavy ions have become the principal tool in nuclear physics research. In order to form a heavy nucleus, a relatively heavier projectile must be fused with heavy target nuclei. This will lead to the formation of a highly excited completely fused system with a reduced probability of survival against fission. Up to now, considerable progress has been achieved in the experimental and theoretical investigations in the region of superheavy elements (SHEs) [1–15]. Several successful [1] experiments have been performed at different laboratories for the production of a SHE with $Z \leqslant 118$, and an attempt to produce $Z = 120$ has been reported [2]. To extend the periodic table, two different experimental approaches to synthesize SHEs are used; the cold fusion reaction performed mainly at the Joint Institute for Nuclear Research-Flerov Laboratory of Nuclear Reactions, Dubna and the hot fusion reaction performed mainly at GSI, Darmstadt and at Rikagaku Kenkyusho, Japan. Using the cold fusion approach, elements with $Z = 107$–112 have been synthesized [4–6], and the hot fusion reaction led to the discoveries of elements with $Z = 113$–118 [7–11]. Several theoretical calculations about the synthesis and decay of SHEs have been performed within the fusion-by-diffusion model [16–18], the nuclear collectivization model [19–20], the dinuclear system model [21–26], and the Coulomb and proximity potentials for deformed nuclei [27–29].

Nuclear theorists have predicted the existence of stability in the upper region of the nuclear chart for the past four decades, and it is called the island of SHEs. The magic number for proton shell closure next to $Z = 82$ is predicted to be at $Z = 114, 120$, and 126 and that of neutron shell closure next to $N = 126$ is commonly predicted to be at $N = 184$ [30–32]. The experimentalists have reached the shore of the island of stability around $Z = 120$, 124, or 126 and $N = 184$ [33] through progress in the accelerator technologies. The study of superheavy element $Z = 120$ is of great interest because it is useful in determining whether the magic proton shell should be at $Z = 114$ or at higher proton numbers of $Z = 120$–126.

The short lifetimes and the low production cross sections (in the region of the SHE, the production cross section is of the order of picobarns) of the SH elements have posed difficulties to both experimentalists and theoreticians in studying the various properties of SH elements. In the calculation of the evaporation residue cross section, the reaction process leading to the synthesis of SHE can be divided into three steps. First, the projectile is captured by the target by overcoming the Coulomb barrier, which then evolves into the compound nucleus, and, finally the compound nucleus loses excitation energy and cools down by the emission of particle and γ rays and goes into the ground state. Therefore, the cross section for producing an evaporation residue σ_{ER} is the product of capture cross section $\sigma_{capture}$, the probability of compound nucleus formation P_{CN}, and the survival probability W_{sur} of the excited compound nucleus [34–36].

For light and medium-heavy projectile-target combinations where the fission barrier is high, each capture event leads to the formation of a compound nucleus, so $\sigma_{capture} \approx \sigma_{fusion} \approx \sigma_{ER}$. But for heavy systems, especially for a more symmetric combination where the fission barrier is comparatively low and

*drkpsanthosh@gmail.com

those leading to superheavy compound nuclei, the quasifission process and the deep inelastic scattering, which lead to the two fragments in the exit channel, come in and compete with the fusion process [35,37]. In this case, only a small part of the capture events are converted to fusion. Hence the complete fusion cross section ($\sigma_{\rm fusion}/\sigma_{\rm CN}$) is a part of the capture cross section $\sigma_{\rm capture}$, and it is necessary to distinguish the capture and fusion processes [38]. The complete fusion cross section can be written as $\sigma_{\rm fusion} = \sigma_{\rm capture}\, P_{\rm CN}$, where $P_{\rm CN}$ is the probability that complete fusion will occur.

In 2008, experiments aimed at the synthesis of isotopes of element $Z = 120$ have been performed using the ^{238}U (^{64}Ni,xn) $^{302-x}$120 reaction, and a cross-sectional limit of 90 fb at $E^* = 36.4$ MeV was obtained [39]. Later in 2009, using the reaction ^{244}Pu (^{58}Fe,xn) $^{302-x}$120, an attempt to produce the $Z = 120$ reaction has been performed, yielding an upper limit of 400 fb [2]. A cross-sectional limit of 560 fb was established in the ^{54}Cr + ^{248}Cm reaction at the search for hidden particles experiment in 2011 [40,41]. From the analysis of mass and total kinetic-energy distributions, compound nucleus fission cross sections were estimated experimentally by Kozulin *et al.* [42] and concluded that the combination of ^{64}Ni + ^{238}U is less favorable to the synthesis element $Z = 120$ compared to the combination of ^{58}Fe + ^{244}Pu.

Several theoretical studies [43–56] are also being performed for investigating the expected cross sections of yet unexplored reactions for the synthesis of new isotopes of element $Z = 120$. Predicted empirical complete fusion cross sections for superheavy element $Z = 120$ for the system ^{252}Cf (^{50}Ti,$4n$) and ^{208}Pb (^{87}Sr,n) by Loveland [43] is 30 and 2 fb, respectively. Zagrebaev and Greiner [44] predicted that excitation functions for the production of the $Z = 120$ element using ^{58}Fe + ^{244}Pu and ^{64}Ni + ^{238}U reactions are lower than those of the less symmetric ^{54}Cr + ^{248}Cm (see Fig. 10 of Ref. [44]). The possibility to synthesis the element $Z = 120$ using ^{50}Ti + $^{249-252}$Cf was evaluated by Liu and Dong Bao [45] within the fusion-by-diffusion model, and it was found that the reactions of ^{250,251}Cf (^{50}Ti,$3n$) ^{297,298}120, and ^{251,252}Cf (^{50}Ti,$4n$) ^{297,298}120 are relatively favorable with the maximum evaporation residue cross sections of 0.12, 0.09, 0.11, and 0.25 pb, respectively. Nasirov *et al.* [49] calculated and compared the fusion and evaporation residue cross sections of ^{50}Ti + ^{249}Cf and ^{54}Cr + ^{248}Cm systems, and it was found that the evaporation residue excitation function for the higher mass asymmetric reaction ^{50}Ti + ^{249}Cf is higher in comparison with the lower mass asymmetric ^{54}Cr + ^{248}Cm. The maximum values of the excitation function of the $3n$ channel of the evaporation residue formation of the above system are about 100 and 55 fb, respectively. Siwek-Wilczynska *et al.* [52] predicted the cross sections for the reactions ^{249}Cf (^{50}Ti,xn) $^{299-x}$120 for which the predicted cross section is only 6 fb. For producing $Z = 120$, the maximum ER cross section obtained by Bao *et al.* [55] is 0.12 pb by the $3n$ channel of ^{50}Ti + ^{251}Cf. The predicted maximum cross section varies greatly, and depending on the models and methods used, the overall uncertainties in predicting the cross section of a SHE is examined by Loveland [56].

The studies on the heavy-ion fusion cross section reveals that, the projectile-target combinations, the incident energy, mass asymmetry in the entrance channel, and excitation energy are the key factors on which the fusion cross sections strongly depend. Hence it will be interesting and useful to study such dependencies for the synthesis of new SHEs. The theoretical predictions will be very useful for the experimentalist to choose the specific combinations with optimum energy and for the estimation of the cross sections. The selection of the most promising projectile-target combination is crucial for an experimentalist for the synthesis of a new element.

One of us (K.P.S.) calculated the total fusion cross sections for the fusion of ^{12}C, ^{16}O, ^{28}Si, and ^{35}Cl on a ^{92}Zr target [57], ^{9}Be on ^{27}Al and ^{64}Zn targets, ^{16}O on a ^{64}Zn target [58], and ^{16}O on a $^{144-154}$Sm target [59] by taking the scattering potential as the sum of the Coulomb and proximity potential [60], and the computed values are compared with experimental data. By using the concept of the cold reaction valley [61], the probable projectile-target combination for ^{286}112 is also studied [62], and it was found that the systems ^{82}Ge + ^{204}Hg, ^{80}Ge + ^{206}Hg, ^{78}Zn + ^{208}Pb, ^{48}Ca + ^{238}U, ^{38}S + ^{248}Cm, and ^{44}Ar + ^{242}Pu in the cold reaction valley are predicted to be the better optimal projectile-target combinations for the synthesis of superheavy nuclei ^{286}112. In the present paper we have studied the cold reaction valley of the ^{302}120 SHE for identifying the better projectile-target combinations for the synthesis of ^{302}120. The scattering potential energy curves for all probable combinations are studied. The probability of the compound nucleus formation $P_{\rm CN}$, the capture cross sections $\sigma_{\rm capture}$, the fusion cross sections $\sigma_{\rm fusion}$, the survival probability $W_{\rm sur}$, and the evaporation residue cross section $\sigma_{\rm ER}$ for the reactions of all the probable projectile-target combinations found in the cold valleys are systematically estimated. The details of the scattering potential and the methodology used in the estimation of the cross sections are described in Sec. II. In Sec. III, results and discussion are given, and the entire work is summarized in Sec. IV.

II. THEORY

A. The potential

The interaction barrier for the two colliding nuclei is given as

$$V = \frac{Z_1 Z_2 e^2}{r} + V_P(z) + \frac{\hbar^2 \ell(\ell+1)}{2\mu r^2}, \tag{1}$$

where Z_1 and Z_2 are the atomic numbers of the projectile and target, r is the distance between the centers of the projectile and target, z is the distance between the near surfaces of the projectile and target, ℓ is the angular momentum, μ is the reduced mass of the target and projectile, and $V_P(z)$ is the proximity potential [63] given as

$$V_P(z) = 4\pi\gamma b \frac{C_1 C_2}{C_1 + C_2} \phi\left(\frac{z}{b}\right), \tag{2}$$

with the nuclear surface tension coefficient,

$$\gamma = 0.9517[1 - 1.7826(N - Z)^2/A^2], \tag{3}$$

ϕ, the universal proximity potential, is given as

$$\phi(\xi) = -4.41\ \exp(-\xi/0.7176) \quad \text{for } \xi \geqslant 1.9475, \tag{4}$$

$$\phi(\xi) = -1.7817 + 0.9270\xi + 0.016\,96\xi^2 - 0.051\,48\xi^3 \quad \text{for } 0 \leqslant \xi \leqslant 1.9475, \tag{5}$$

$$\phi(\xi) = -1.7817 + 0.9270\xi + 0.0143\xi^2 - 0.09\xi^3 \quad \text{for } \xi \leqslant 0. \tag{6}$$

Here $\xi = z/b$ where the width (diffuseness) of the nuclear surface is $b \approx 1$ fm and the Siissmann central radii C_i are related to sharp radii R_i as $C_i = R_i - \frac{b^2}{R_i}$.

For R_i, we use the semiempirical formula in terms of mass number A_i as

$$R_i = 1.28{A_i}^{1/3} - 0.76 + 0.8{A_i}^{-1/3}. \tag{7}$$

B. Cross section

1. Capture or total cross section

To describe the fusion reactions at energies not too much above the barrier and at higher energies, the barrier penetration model developed by Wong [64] has been widely used, which obviously explains the experimental result properly.

The capture cross section at a given center-of-mass energy E can be written as the sum of the cross section for each partial wave ℓ,

$$\sigma_{\text{capture}} = \frac{\pi}{k^2}\sum_{\ell=0}^{\infty}(2\ell+1)T(E,\ell), \tag{8}$$

where $T(E,\ell)$ denotes the penetration probability of the ℓth partial wave, $k = \sqrt{\frac{2\mu E}{\hbar^2}}$, and μ is the reduced mass of the interacting system.

Following Thomas [65], Huizenga and Igo [66], and Rasmussen and Sugawara-Tanabe [67], Wong [64] approximated the various barriers for different partial waves by inverted harmonic-oscillator potentials of height E_ℓ and frequency ω_ℓ. For energy E, the probability for the absorption of the ℓ^{th} partial wave given by the Hill-Wheeler formula [68] is

$$T(E,\ell) = \{1 + \exp[2\pi(E_\ell - E)/\hbar\omega_\ell]\}^{-1}. \tag{9}$$

In consequence, Wong arrived at the total cross section for the fusion of two nuclei, and it is given by

$$\sigma_{\text{capture}} = \frac{\pi}{k^2}\sum_{\ell}\frac{2\ell+1}{1+\exp[2\pi(E_\ell - E)/\hbar\omega_\ell]}. \tag{10}$$

Here $\hbar\omega_\ell$ is the curvature of the inverted parabola. Using some parametrizations in the region $\ell = 0$ and replacing the sum in Eq. (8) by an integral, Wong gave the reaction cross section as

$$\sigma_{\text{capture}} = \frac{R_0^2\hbar\omega_0}{2E}\ln\left\{1+\exp\left[\frac{2\pi(E-E_0)}{\hbar\omega_0}\right]\right\}, \tag{11}$$

where R_0 is the barrier radius and E_0 is the barrier height for $\ell = 0$.

The barrier radius for $\ell = 0$ is obtained from the condition,

$$\left.\frac{dV(r)}{dr}\right|_{R_0} = 0. \tag{12}$$

The curvature $\hbar\omega_0$ is related to the potential given by

$$\hbar\omega_0 = \frac{\hbar}{\sqrt{\mu}}\sqrt{\left.\frac{d^2V(r)}{dr^2}\right|_{R_0}}. \tag{13}$$

For relatively large values of E, the above result reduces to the well-known formula,

$$\sigma_{\text{capture}} = \pi R_0^2\left[1 - \frac{E_0}{E}\right]. \tag{14}$$

Galin and collaborators have shown that not a critical angular momentum but a critical distance of the approach may be the relevant quantity limiting complete fusion during a collision between two complex nuclei [69]. In order to substantiate the finding of a critical distance of approach, it is necessary to check the linear dependence of σ on $1/E$ in the region of high energy. The value of critical distance was found to be

$$R_C = r_C\left(A_1^{1/3} + A_2^{1/3}\right), \quad r_C = 1.0 \pm 0.07 \text{ fm}. \tag{15}$$

Gutbrod *et al.* from their analysis of low-energy data [70] obtain the fusion distance as

$$R_B = r_B\left(A_1^{1/3} + A_2^{1/3}\right), \quad r_B = 1.4 \text{ fm}, \tag{16}$$

that is 40% larger than the value of R_C and corresponds to the distance of the ions at the fusion barrier. In order to understand the difference between the two distances given by Eqs. (15) and (16), Glas and Mosel [71] set the cross section as

$$\sigma_{\text{capture}} = \frac{\pi}{k^2}\sum_{\ell=0}^{\infty}(2\ell+1)T_\ell P_\ell, \tag{17}$$

where T_ℓ is the penetration probability and $P_\ell = 1$ for $\ell \leqslant \ell_c$; $P_\ell = 0$ for $\ell > \ell_c$.

Replacing the sum in Eq. (17) by an integration, one obtains

$$\sigma_{\text{capture}} = \frac{R_B^2\hbar\omega}{2}\frac{1}{E}\ln\left\{\frac{1+\exp\{2\pi[E - V(R_B)]/\hbar\omega\}}{1+\exp\left(2\pi\{E - V(R_B) - (R_C/R_B)^2[E - V(R_C)]\}/\hbar\omega\right)}\right\}, \tag{18}$$

where $V(R_B)$ and $V(R_C)$ are the barrier heights corresponding to R_B and R_C, respectively.

2. Fusion cross section

We observe that the complete fusion cross section constitutes only a small fraction of the capture cross section, especially for the heavier targets and is always smaller or equal to the capture cross section.

The fusion cross section is expressed as

$$\sigma_{\text{fusion}} = \frac{\pi}{k^2}\sum_{\ell=0}^{\infty}(2\ell+1)T(E,\ell)P_{\text{CN}}(E,\ell), \tag{19}$$

where P_{CN} is the probability of compound nucleus formation, which is described in the next section.

Probability of compound nucleus formation P_{CN}. Different models and empirical formulas [43,44,72–82] have been proposed for the calculation of the most unclear part P_{CN}, and there is no satisfactory quantitative model for the fusion probability.

Armbruster [73] has suggested

$$P_{CN}(E,\ell) = 0.5\ \exp\left[-c(x_{eff} - x_{thr})\right]. \tag{20}$$

The studies [43,44,74,79] have found that there exists beam energy dependence for the fusion probability.

The energy dependent fusion probability is used by us to calculate P_{CN} and is given by

$$P_{CN}(E,\ell) = \frac{\exp\{-c(x_{eff} - x_{thr})\}}{1 + \exp\left\{\frac{E_B^* - E^*}{\Delta}\right\}}, \tag{21}$$

where E^* is the excitation energy of the compound nucleus, E_B^* denotes the excitation energy of the CN when the center-of-mass beam energy is equal to the Coulomb and proximity barrier, Δ is an adjustable parameter ($\Delta = 4$ MeV), and x_{eff} is the effective fissility defined as

$$x_{eff} = \left[\frac{(Z^2/A)}{(Z^2/A)_{crit}}\right][1 - \alpha + \alpha f(k)], \tag{22}$$

with $(Z^2/A)_{crit}$, $f(k)$, and k given by

$$(Z^2/A)_{crit} = 50.883\left[1 - 1.7286\left(\frac{(N-Z)}{A}\right)^2\right], \tag{23}$$

$$f(k) = \frac{4}{K^2 + K + \frac{1}{k} + \frac{1}{k^2}}, \tag{24}$$

$$k = (A_1/A_2)^{1/3}, \tag{25}$$

where Z, N, and A represent the atomic number, neutron number, and mass number, respectively. A_1 and A_2 are the mass number of the projectile and target, respectively. x_{thr} and c are adjustable parameters, and $\alpha = 1/3$. For the best fit to the cold fusion reaction, the values of c and x_{eff} are 136.5 and 0.79, respectively. For the hot fusion reaction, the best fit for $x_{eff} \leqslant 0.8$ is $c = 104$ and $x_{thr} = 0.69$; whereas for $x_{eff} \geqslant 0.8$, the values are $c = 82$ and $x_{thr} = 0.69$. These constants are suggested by Loveland [43]. This form of energy dependence of fusion probability is similar to the one proposed by Zargrebeav and Greiner [44].

3. Evaporation residue cross section

The cross section of SH element production in a heavy-ion fusion reaction with subsequent emission of x neutrons is given by

$$\sigma_{ER}^{xn} = \frac{\pi}{k^2}\sum_{\ell=0}^{\infty}(2\ell+1)T(E,\ell)P_{CN}(E,\ell)W_{sur}^{xn}(E^*,\ell). \tag{26}$$

W_{sur} is the probability for the compound nucleus to decay to the ground state of the final residual nucleus via evaporation of light particles and a γ ray for avoiding the fission process and is described in the next section.

Survival probability W_{sur}. The survival probability is the probability that the fused system emits several neutrons followed by observing a sequence of α decay from the residue. The survival probability under the evaporation of x neutrons is

$$W_{sur} = P_{xn}(E_{CN}^*)\prod_{i=1}^{i_{max}=x}\left(\frac{\Gamma_n}{\Gamma_n + \Gamma_f}\right)_{i,E^*}, \tag{27}$$

where the index "i" is equal to the number of emitted neutrons, P_{xn} is the probability of emitting exactly x neutrons [83], E^* is the excitation energy of the compound nucleus, and Γ_n and Γ_f represent the decay width of neutron evaporation and fission, respectively. To calculate Γ_n/Γ_f, Vandenbosch and Huizenga [84] have suggested a classical formalism,

$$\frac{\Gamma_n}{\Gamma_f} = \frac{4A^{2/3}a_f(E^* - B_n)}{K_0 a_n[2a_f^{1/2}(E^* - B_f)^{1/2} - 1]} \times \exp\left[2a_n^{1/2}(E^* - B_n)^{1/2} - 2a_f^{1/2}(E^* - B_f)^{1/2}\right], \tag{28}$$

where A is the mass number of the nucleus considered, E^* is the excitation energy, and B_n is the neutron separation energy. The constant K_0 is taken as 10 MeV. $a_n = A/10$ and $a_f = 1.1a_n$ are the level density parameters of the daughter nucleus and the fissioning nucleus at the ground state and saddle configurations, respectively. B_f is the fission barrier, and this height is a decisive quantity in the competition between processes of neutron evaporation and fission of the compound nucleus in the process of its cooling to form a residual nucleus in its ground state.

III. RESULTS AND DISCUSSION

The driving potential, which is the difference between the interaction potential (Coulomb and proximity potential) and the Q value of the reaction for all the projectile target combinations of the SHE $^{302}120$ is calculated. For a fixed pair of (A_P, A_T), a pair of (Z_P, Z_T) is singled out for which the driving potential is minimum and is plotted as a function of projectile mass number A_P. This plot is usually referred to as the cold reaction valley plot and is shown in Fig. 1. The minima and deep minima valleys in these plots correspond to the magicity of projectile and target combinations, and these minima represent the most probable projectile-target combinations for fusion of a superheavy element.

In the cold reaction valleys of the superheavy element $^{302}120$, the probable combinations observed are ^{8}Be + ^{294}Lv, ^{10}Be + ^{292}Lv, ^{12}C + ^{290}Fl, ^{14}C + ^{288}Fl, ^{16}C + ^{286}Fl, ^{20}O + ^{282}Cn, ^{22}O + ^{280}Cn, ^{24}Ne + ^{278}Ds, ^{26}Ne + ^{276}Ds, ^{28}Mg + ^{274}Hs, ^{30}Mg + ^{272}Hs, ^{32}Si + ^{270}Sg, ^{34}Si + ^{268}Sg, ^{36}Si + ^{266}Sg, ^{38}S + ^{264}Rf, ^{40}S + ^{262}Rf, ^{42}S + ^{260}Rf, etc. The three deep minima are observed in the range of $44 < A_P < 60$ (region I), $84 < A_P < 100$ (region II), and $126 < A_P < 138$ (region III), which are due to the magic shell closures of either or both of the interacting nuclei. The probable combinations observed in region I of the cold valley plot are ^{44}Ar + ^{258}No, ^{46}Ar + ^{256}No, ^{48}Ca + ^{254}Fm, ^{50}Ca + ^{252}Fm, ^{52}Ca + ^{250}Fm, ^{54}Ti + ^{248}Cf, ^{56}Ti + ^{246}Cf, ^{58}Cr + ^{244}Cm, and ^{60}Cr + ^{242}Cm; in region II, the combinations are

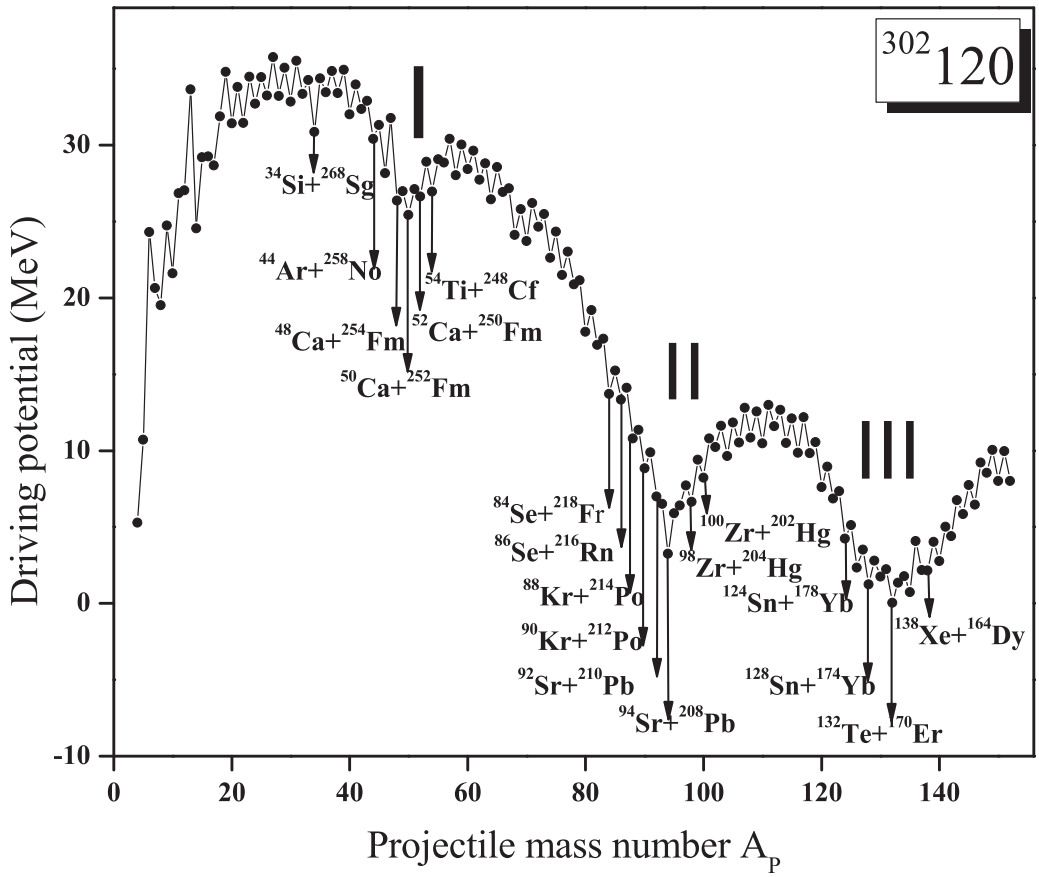

FIG. 1. Cold reaction valley plot for the superheavy nucleus $^{302}120$.

$^{84}Se + ^{218}Rn$, $^{86}Se + ^{216}Rn$, $^{88}Kr + ^{214}Po$, $^{90}Kr + ^{212}Po$, $^{92}Sr + ^{210}Pb$, $^{94}Sr + ^{208}Pb$, $^{96}Sr + ^{206}Pb$, and $^{98}Zr + ^{204}Hg$; and in region III, the combinations are $^{124}Sn + ^{178}Yb$, $^{126}Sn + ^{176}Yb$, $^{128}Sn + ^{174}Yb$, and $^{130}Te + ^{172}Er$.

In region I, the minima at $^{46}Ar + ^{256}No$ are due to the neutron shell closure $N = 28$ of ^{46}Ar, and the minima at $^{48}Ca + ^{254}Fm$, $^{50}Ca + ^{252}Fm$, and $^{52}Ca + ^{250}Fm$ are due to the presence of doubly or near-doubly magic nuclei Ca. The combinations $^{92}Sr + ^{210}Pb$, $^{94}Sr + ^{208}Pb$, and $^{96}Sr + ^{206}Pb$ in region II are because of doubly or near-doubly magic nuclei Pb, and in region III, the combinations $^{124}Sn + ^{178}Yb$, $^{126}Sn + ^{176}Yb$, $^{128}Sn + ^{174}Yb$, $^{130}Te + ^{172}Er$, and $^{132}Te + ^{170}Er$ were observed due to near-doubly magic nuclei Sn and Te and make these systems suitable projectile-target combinations for the synthesis of the superheavy nucleus $^{302}120$. Since the above discussed combinations lie in the cold valleys, they are the optimal cases of binary splitting and hence can be identified as the optimal projectile-target combinations for the synthesis of a superheavy element with considerations to the nature of the interaction barrier, potential pocket, and the probability of CN formation.

For all the optimal projectile-target combinations identified in the cold valley of the superheavy $^{302}120$ nucleus using the Coulomb and proximity potential as the scattering potential, we have studied the interaction barriers (scattering potential-energy curve) for the fusion of the projectile and target against the distance among the centers of the colliding nuclei and the corresponding barrier height V_B, the barrier radius R_B, and the quasifission barrier B_{qf} (depth of the potential well in the nucleus-nucleus interaction) is noted with $\ell = 0$, and the values are given in Table I. While analyzing the interaction barrier, it was found that barrier height V_B is increasing and the quasifission barrier is decreasing with an increasing atomic number of the projectile.

As the part of a systematic study for predicting the most suitable projectile-target combination for heavy-ion fusion experiments in the synthesis of $^{302}120$, initially considered the projectile-target combinations $^{126}Sn + ^{176}Yb$, $^{128}Sn + ^{174}Yb$, $^{130}Te + ^{172}Er$, and $^{132}Te + ^{170}Er$, which were found in deep region III of the cold valleys of $^{302}120$. The interaction barrier against the distance between the centers of the projectile and target for the above four combinations are shown in Fig. 2. But, while observing Fig. 2, it is clear that the quasifission barrier that are to be appreciable for fusion to take place are shallow in all four cases and hence cannot be used as a suitable projectile-target combination for heavy-ion fusion reactions. Moreover, the projectiles are comparatively heavy, systems are nearly symmetric, and for those systems leading to the SHE $^{302}120$, the quasifission and deep inelastic scattering compete with the fusion process with a reduced probability of forming CN. So combinations in region III are not favorable for fusion.

While analyzing the interaction barriers for the rest of the combinations in the cold valley, it is observed that the

TABLE I. Barrier height V_B, barrier radius R_B, and quasifission barrier height $B_{\rm qf}$ for the systems in the cold reaction valleys of $^{302}120$ nuclei taking the Coulomb and proximity potential as the interacting barrier.

Reaction	Barrier height V_B (MeV)	Barrier radius R_B (fm)	Quasifission barrier $B_{\rm qf}$ (MeV)	Reaction	Barrier height V_B (MeV)	Barrier radius R_B (fm)	Quasifission barrier $B_{\rm qf}$ (MeV)
^{8}Be + ^{294}Lv	51.214	12.300	19.786	^{56}Ti + ^{246}Cf	219.328	13.343	7.688
^{10}Be + ^{292}Lv	50.279	12.430	24.283	^{58}Cr + ^{244}Cm	234.671	13.206	5.652
^{12}C + ^{290}Fl	74.756	12.375	17.143	^{60}Cr + ^{242}Cm	233.940	13.269	6.210
^{14}C + ^{288}Fl	73.764	12.585	21.143	^{62}Fe + ^{240}Pu	248.440	13.146	4.188
^{16}C + ^{286}Fl	72.897	12.708	24.648	^{64}Fe + ^{238}Pu	247.714	13.190	4.507
^{20}O + ^{282}Cn	95.119	12.749	21.076	^{66}Fe + ^{236}Pu	247.050	13.300	5.341
^{22}O + ^{280}Cn	94.316	12.921	23.355	^{68}Ni + ^{234}U	260.650	13.163	3.513
^{24}Ne + ^{278}Ds	116.278	12.837	18.055	^{70}Ni + ^{232}U	259.960	13.217	4.188
^{26}Ne + ^{276}Ds	115.418	12.922	19.850	^{72}Ni + ^{230}U	259.367	13.320	4.507
^{28}Mg + ^{274}Hs	136.364	12.889	15.037	^{74}Zn + ^{228}Th	272.110	13.210	2.839
^{30}Mg + ^{272}Hs	135.497	12.983	16.455	^{76}Zn + ^{226}Th	271.470	13.246	3.407
^{32}Si + ^{270}Sg	155.440	12.943	12.533	^{78}Ge + ^{224}Ra	283.464	13.149	2.061
^{34}Si + ^{268}Sg	154.551	13.012	13.940	^{80}Ge + ^{222}Ra	282.813	13.146	2.444
^{36}Si + ^{266}Sg	153.748	13.103	15.150	^{82}Ge + ^{220}Ra	282.223	13.244	2.825
^{38}S + ^{264}Rf	172.685	13.042	11.409	^{84}Se + ^{218}Rn	293.808	13.198	1.867
^{40}S + ^{262}Rf	171.860	13.128	12.530	^{86}Se + ^{216}Rn	292.808	13.216	2.163
^{42}S + ^{260}Rf	171.075	13.180	13.490	^{88}Kr + ^{214}Po	303.174	13.118	0.721
^{44}Ar + ^{258}No	189.080	13.127	11.178	^{90}Kr + ^{212}Po	302.644	13.192	0.874
^{46}Ar + ^{256}No	188.282	13.176	10.216	^{92}Sr + ^{210}Pb	312.046	13.028	0.493
^{48}Ca + ^{254}Fm	205.389	13.120	8.174	^{94}Sr + ^{208}Pb	311.499	13.051	0.577
^{50}Ca + ^{252}Fm	204.603	13.175	9.105	^{98}Zr + ^{204}Hg	319.803	12.992	0.294
^{52}Ca + ^{250}Fm	203.873	13.259	9.867	^{100}Zr + ^{202}Hg	319.312	13.060	0.458
^{54}Ti + ^{248}Cf	220.070	13.200	7.223	^{102}Zr + ^{200}Hg	318.847	13.083	0.478

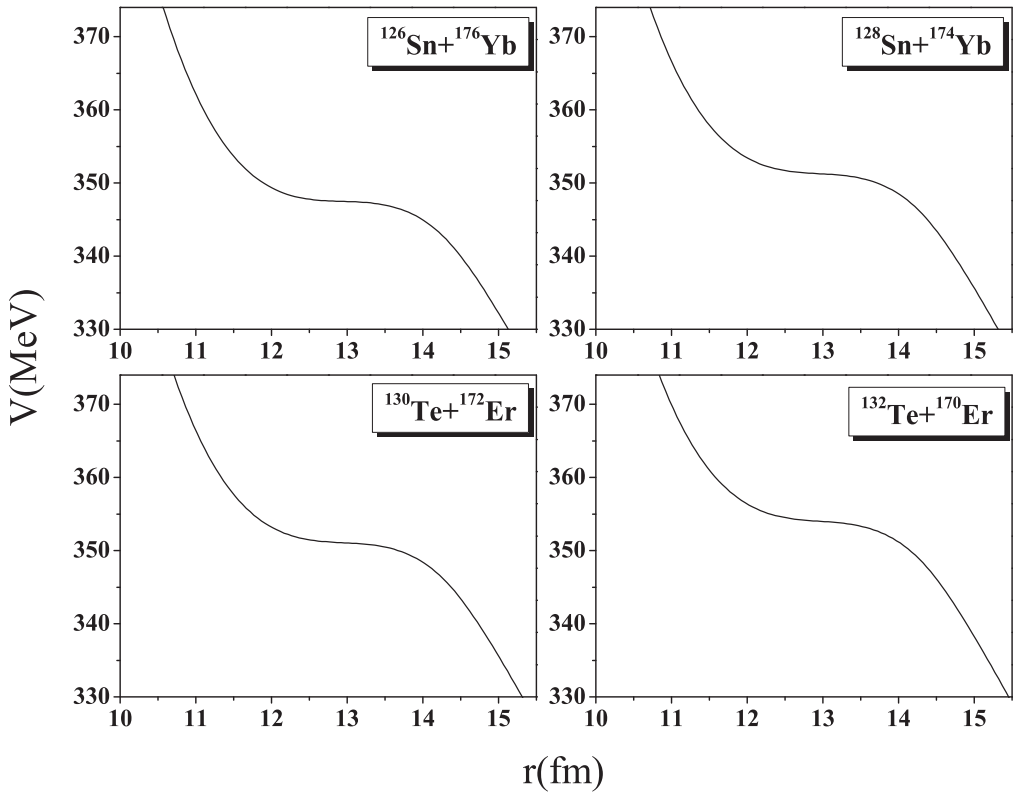

FIG. 2. Scattering potential for the reactions of ^{126}Sn + ^{176}Yb, ^{128}Sn + ^{174}Yb, ^{130}Te + ^{172}Er, and ^{132}Te + ^{170}Er.

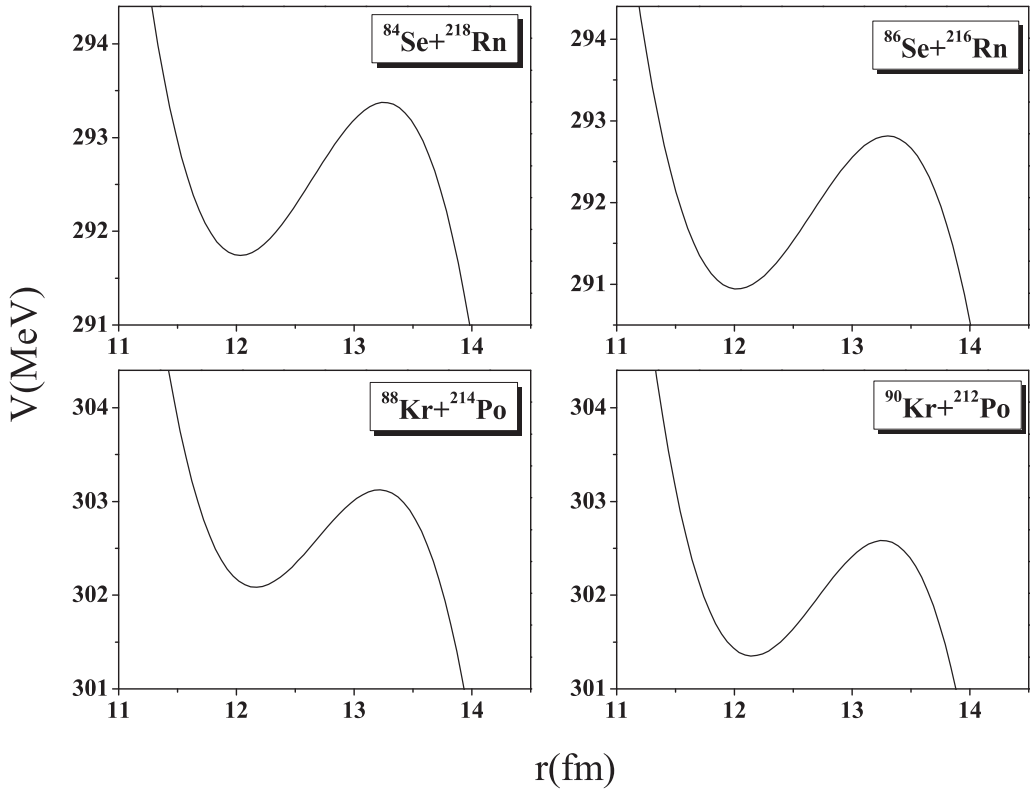

FIG. 3. Scattering potential for the reactions of $^{84}\mathrm{Se}+{}^{218}\mathrm{Rn}$, $^{86}\mathrm{Se}+{}^{216}\mathrm{Rn}$, $^{88}\mathrm{Kr}+{}^{214}\mathrm{Po}$, and $^{90}\mathrm{Kr}+{}^{212}\mathrm{Po}$.

potential pocket is observed only for the combinations up to the $^{102}\mathrm{Zr}+{}^{200}\mathrm{Hg}$ system. The barrier height V_B, the barrier radius R_B, and the potential pocket for the $^{102}\mathrm{Zr}+{}^{200}\mathrm{Hg}$ system are 318.847 MeV, 13.083 fm, and 478 eV respectively. It is noted that, from the interaction barrier for the combinations $^{84}\mathrm{Se}+{}^{218}\mathrm{Rn}$, $^{86}\mathrm{Se}+{}^{216}\mathrm{Rn}$, $^{88}\mathrm{Kr}+{}^{214}\mathrm{Po}$, $^{90}\mathrm{Kr}+{}^{212}\mathrm{Po}$ (shown in Fig. 3), $^{92}\mathrm{Sr}+{}^{210}\mathrm{Pb}$, $^{94}\mathrm{Sr}+{}^{208}\mathrm{Pb}$, $^{96}\mathrm{Sr}+{}^{206}\mathrm{Pb}$, and $^{98}\mathrm{Zr}+{}^{204}\mathrm{Hg}$ (shown in Fig. 4) found in region II, the potential pocket is small compared with that for the combinations $^{44}\mathrm{Ar}+{}^{258}\mathrm{No}$, $^{46}\mathrm{Ar}+{}^{256}\mathrm{No}$, $^{48}\mathrm{Ca}+{}^{254}\mathrm{Fm}$, $^{50}\mathrm{Ca}+{}^{252}\mathrm{Fm}$ (shown in Fig. 5), $^{52}\mathrm{Ca}+{}^{250}\mathrm{Fm}$, $^{54}\mathrm{Ti}+{}^{248}\mathrm{Cf}$, $^{56}\mathrm{Ti}+{}^{246}\mathrm{Cf}$, and $^{58}\mathrm{Cr}+{}^{244}\mathrm{Cm}$ (shown in Fig. 6) found in region I. The potential pocket is appreciable in the cases of combinations found in cold valley region I and that of combinations in region II. So, combinations in the first deep region and the second deep region can be identified as the most probable projectile-target combinations for fusion. Excitation energy of the combinations in region I near and above the barrier is comparatively higher than that in region II because combinations in region I are more asymmetric. So we can take combinations in region I as favorable for a hot fusion reaction, and the combinations in region II are favorable for cold fusion reactions.

Furthermore, in an attempt to predict more suitable projectile-targets, which have good potential pockets, we have considered the projectiles and targets having comparatively large half-lives and the systems $^{20}\mathrm{O}+{}^{282}\mathrm{Cn}$, $^{36}\mathrm{Si}+{}^{266}\mathrm{Sg}$, $^{40}\mathrm{S}+{}^{262}\mathrm{Rf}$, $^{62}\mathrm{Fe}+{}^{240}\mathrm{Pu}$, $^{64}\mathrm{Fe}+{}^{238}\mathrm{Pu}$, $^{66}\mathrm{Fe}+{}^{236}\mathrm{Pu}$, $^{68}\mathrm{Ni}+{}^{234}\mathrm{U}$, $^{70}\mathrm{Ni}+{}^{232}\mathrm{U}$, $^{72}\mathrm{Ni}+{}^{230}\mathrm{U}$, and $^{74}\mathrm{Zn}+{}^{228}\mathrm{Th}$ found in the other cold valley are also feasible for fusion experiments. It is noted that, as the reaction asymmetry increases, excitation energy also increases. The excitation energy near and above the barrier for the combinations $^{20}\mathrm{O}+{}^{282}\mathrm{Cn}$, $^{36}\mathrm{Si}+{}^{266}\mathrm{Sg}$, and $^{40}\mathrm{S}+{}^{262}\mathrm{Rf}$, which are more mass asymmetric than the combinations in region I, is comparatively higher and thus has less survival probability to form an evaporation residue and these combinations are not at all favorable for fusion. Based on the two simple arguments of reaction asymmetry and excitation energy, the combinations $^{20}\mathrm{O}+{}^{282}\mathrm{Cn}$, $^{36}\mathrm{Si}+{}^{266}\mathrm{Sg}$, and $^{40}\mathrm{S}+{}^{262}\mathrm{Rf}$ are not promising choices for an attempt to synthesize the element $^{302}120$.

We have evaluated the capture cross sections as a function of center-of-mass energy (excitation function) for the predicted combinations using the Wong formula [64], the approximated Wong formula [64], and the Glas and Mosel formula [71]. The corresponding excitation function $\sigma_{\mathrm{capture}}$ versus E_{cm} are given in the upper panels of Figs. 14–25. It is found that the Wong formula is in good agreement with the Glas and Mosel formula [71].

In order to find the fusion cross section for these combinations of superheavy $^{302}120$, the knowledge of probability of the compound nucleus formation P_{CN} is a must, is determined using Eq. (21), and is plotted against the excitation energy of the compound nucleus which is shown in Figs. 7–12. It is found that P_{CN} for the combinations in region II (less asymmetric cold combinations) is very small as compared to combinations in region I (more asymmetric hot combination). It is found that P_{CN} is larger for the more asymmetric hot combination. For a given excitation energy ($E^* = 35$ MeV

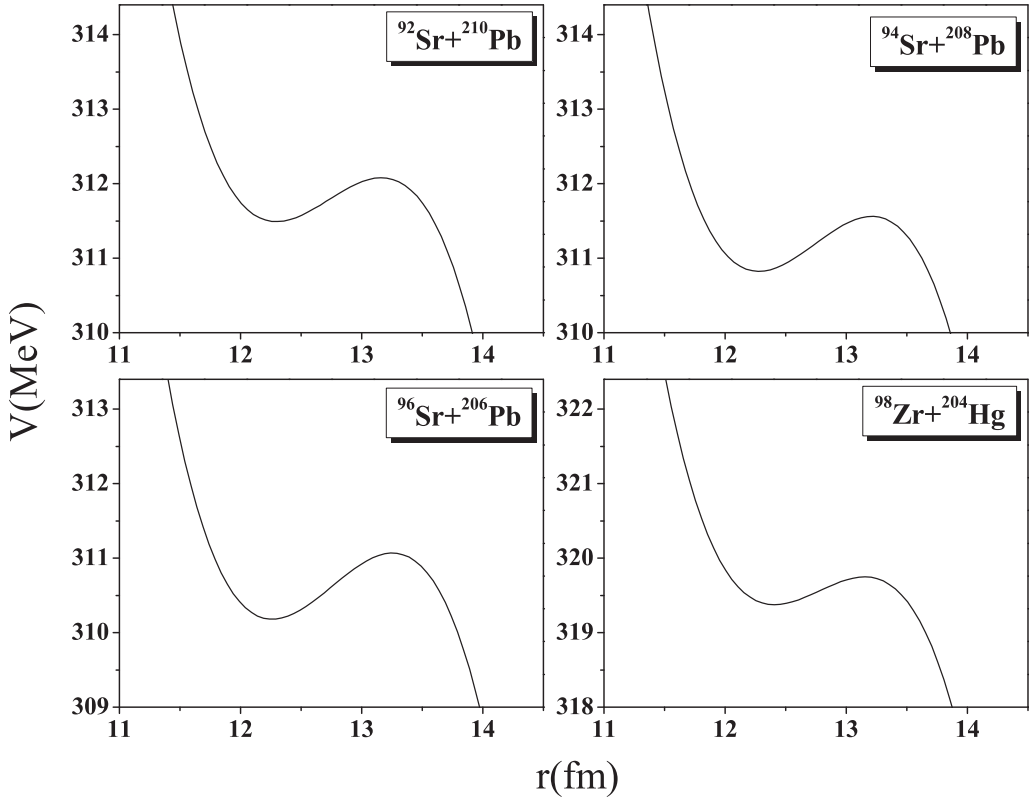

FIG. 4. Scattering potential for the reactions of $^{92}\mathrm{Sr} + {}^{210}\mathrm{Pb}$, $^{94}\mathrm{Sr} + {}^{208}\mathrm{Pb}$, $^{96}\mathrm{Sr} + {}^{206}\mathrm{Pb}$, and $^{98}\mathrm{Zr} + {}^{204}\mathrm{Hg}$.

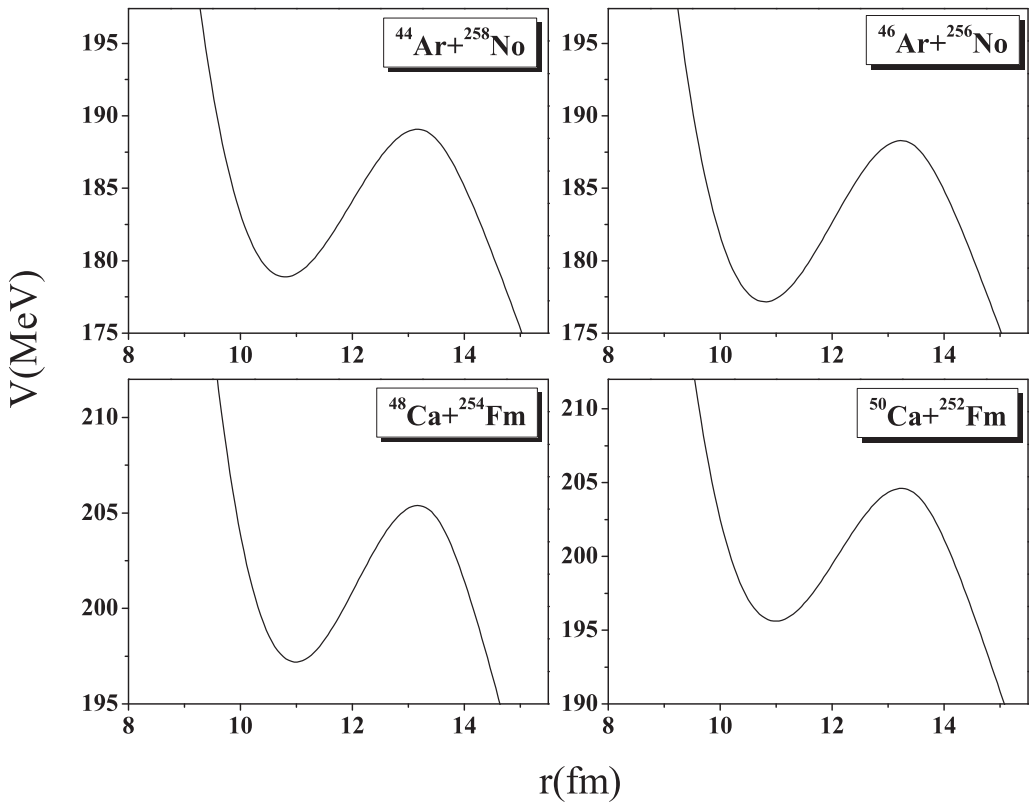

FIG. 5. Scattering potential for the reactions of $^{44}\mathrm{Ar} + {}^{258}\mathrm{No}$, $^{46}\mathrm{Ar} + {}^{256}\mathrm{No}$, $^{48}\mathrm{Ca} + {}^{254}\mathrm{Fm}$, and $^{50}\mathrm{Ca} + {}^{252}\mathrm{Fm}$.

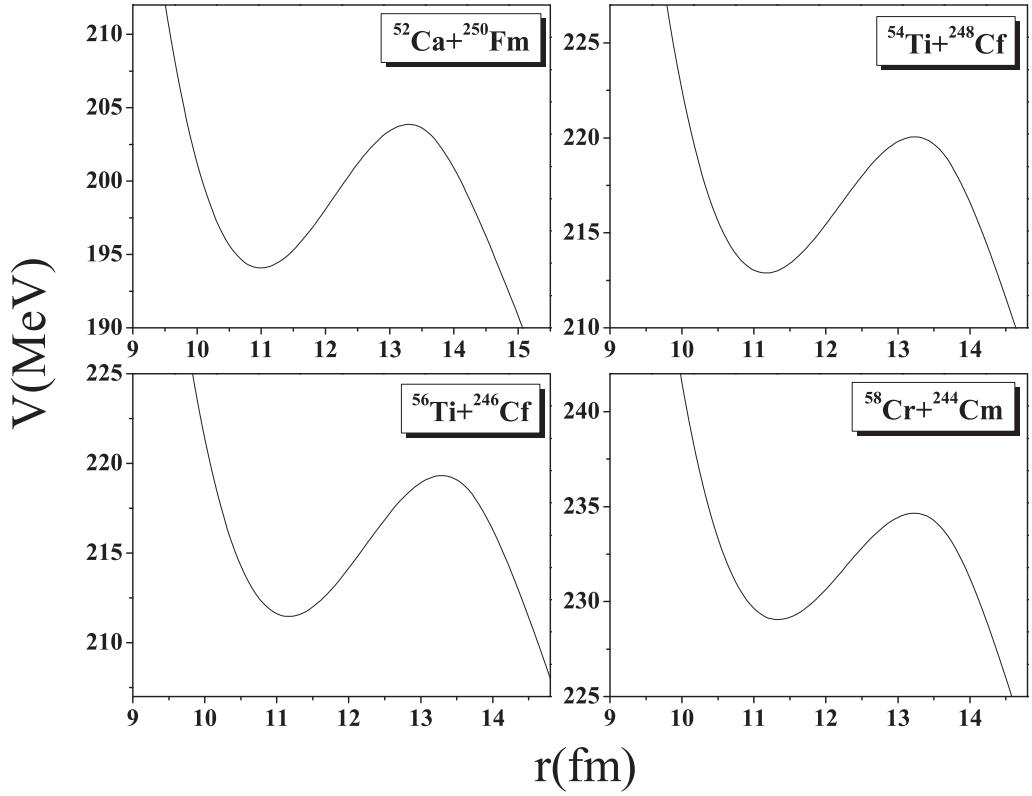

FIG. 6. Scattering potential for the reactions of ^{52}Ca + ^{250}Fm, ^{54}Ti + ^{248}Cf, ^{56}Ti + ^{246}Cf, and ^{58}Cr + ^{244}Cm.

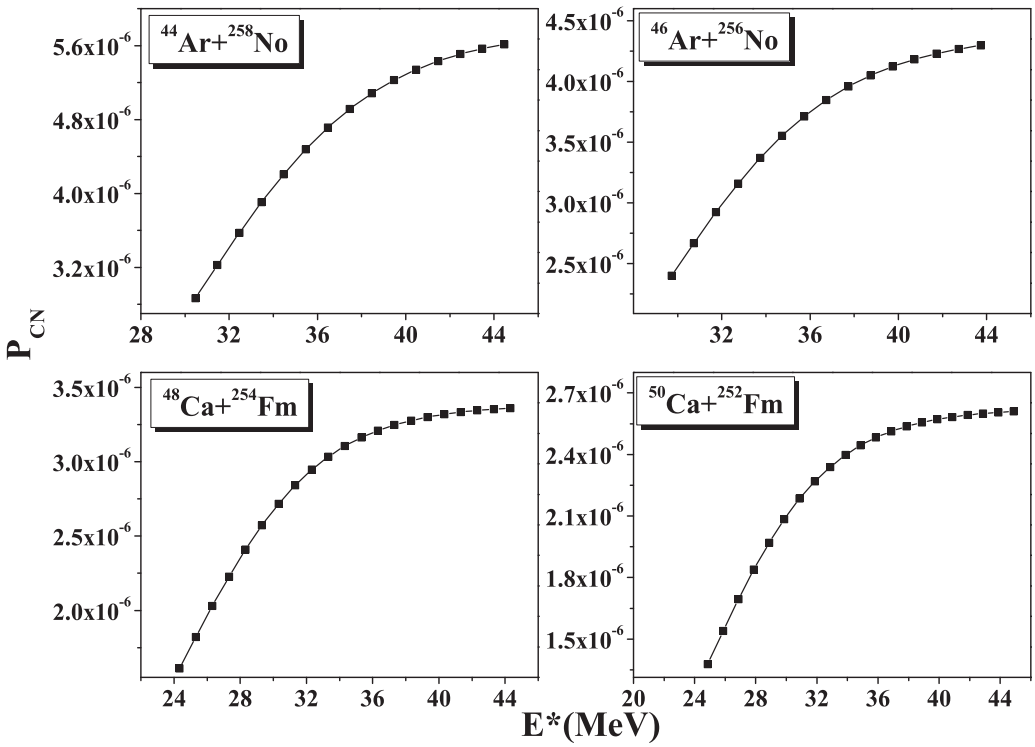

FIG. 7. The plot of P_{CN} versus E^* in MeV for the reactions of ^{44}Ar + ^{258}No, ^{46}Ar + ^{256}No, ^{48}Ca + ^{254}Fm, and ^{50}Ca + ^{252}Fm.

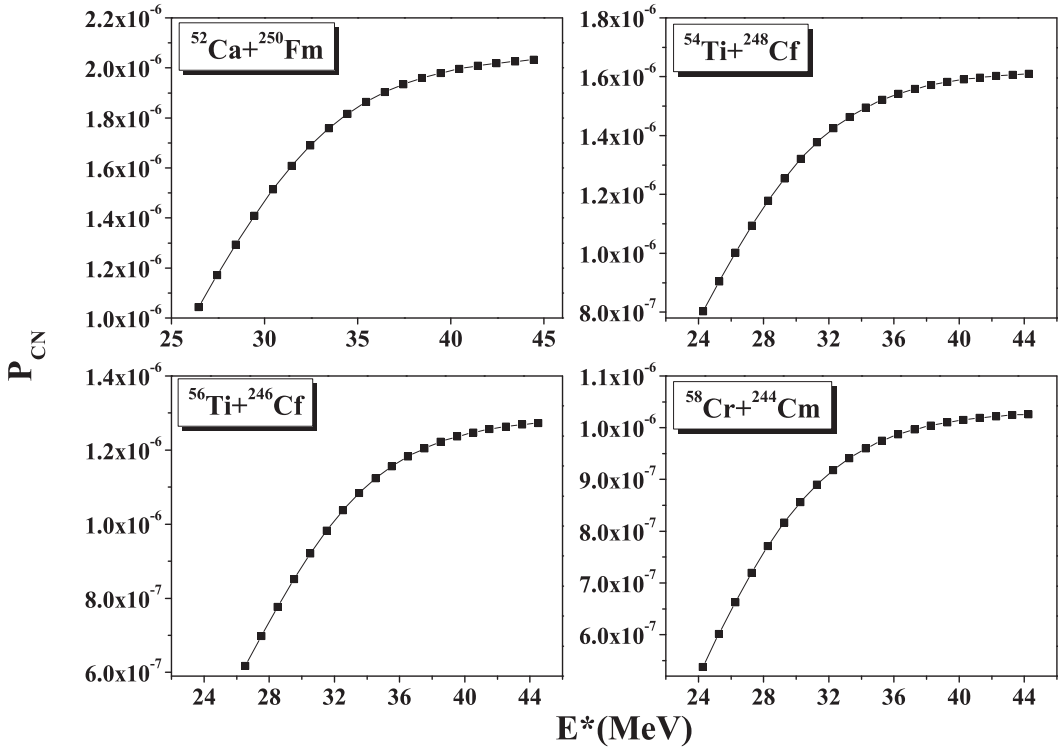

FIG. 8. The plot of P_{CN} versus E^* in MeV for the reactions of $^{52}Ca + ^{250}Fm$, $^{54}Ti + ^{248}Cf$, $^{56}Ti + ^{246}Cf$, and $^{58}Cr + ^{244}Cm$.

for the hot fusion reaction and $E^* = 5$ MeV for the cold fusion reaction), it can also be seen from Fig. 13 that P_{CN} is larger for the more asymmetric hot fusion combinations. Fusion probability increases with increasing the quasifission barrier height (potential pocket) and the incident energies in the reactions leading to the SHE.

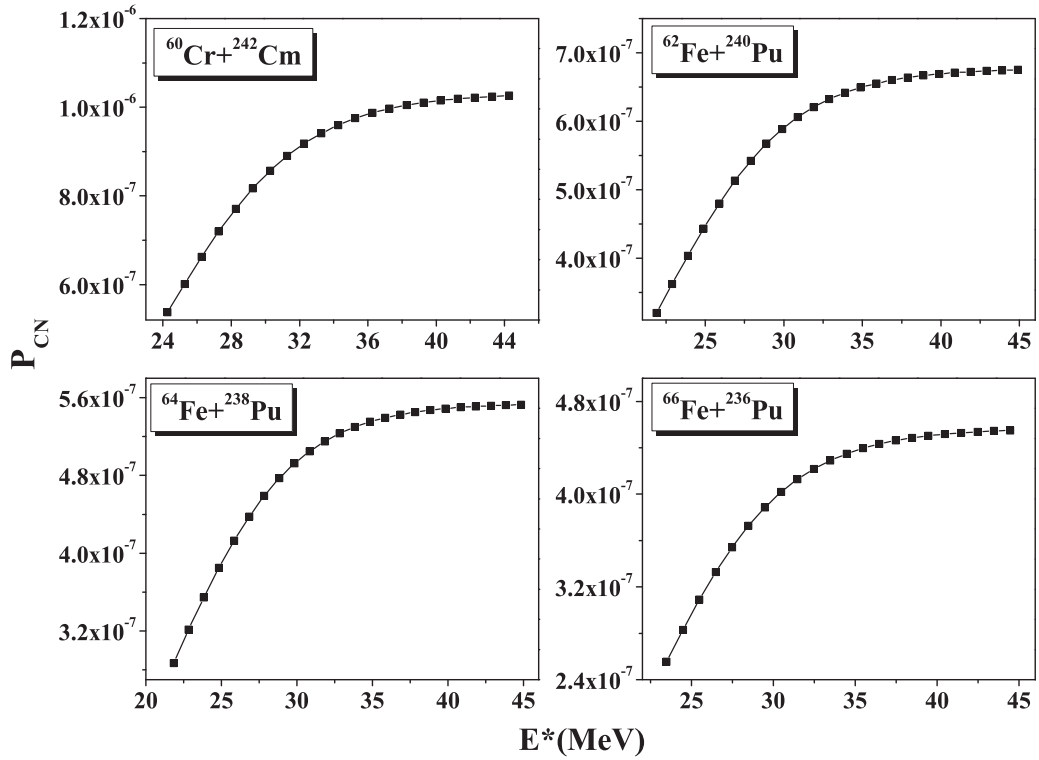

FIG. 9. The plot of P_{CN} versus E^* in MeV for the reactions of $^{60}Cr + ^{242}Cm$, $^{62}Fe + ^{240}Pu$, $^{64}Fe + ^{238}Pu$, and $^{66}Fe + ^{236}Pu$.

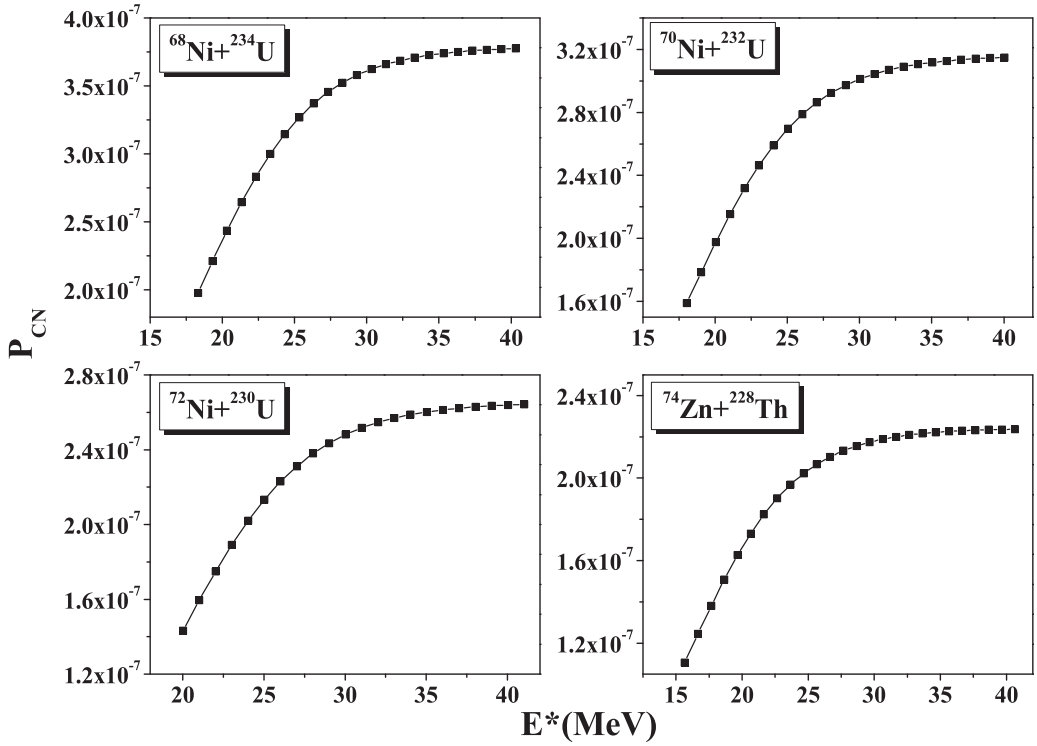

FIG. 10. The plot of P_{CN} versus E^* in MeV for the reactions of ^{68}Ni + ^{234}U, ^{70}Ni + ^{232}U, ^{72}Ni + ^{230}U, and ^{74}Zn + ^{228}Th.

Near and above the barrier, using the values of P_{CN} for each center-of-mass energy, the fusion cross section is computed by using the equation $\sigma_{fusion} = \sigma_{capture\,X} P_{CN}$ for the above systems, and the corresponding fusion excitation functions (σ_{fusion} versus E_{cm} plots) are shown in the upper panels of Figs. 14–25. From the plots it can be seen that the computed fusion cross section for combinations in the first deep region $44 < A_P < 58$ is of the order of microbarns,

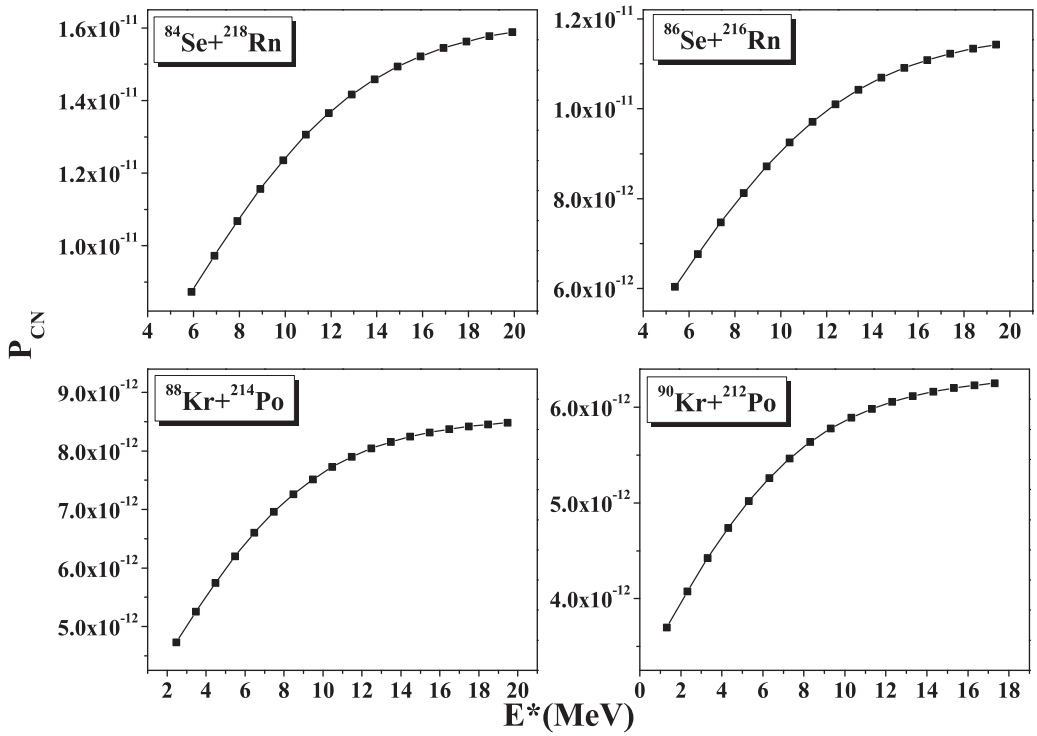

FIG. 11. The plot of P_{CN} versus E^* in MeV for the reactions of ^{84}Se + ^{218}Rn, ^{86}Se + ^{216}Rn, ^{88}Kr + ^{214}Po, and ^{90}Kr + ^{212}Po.

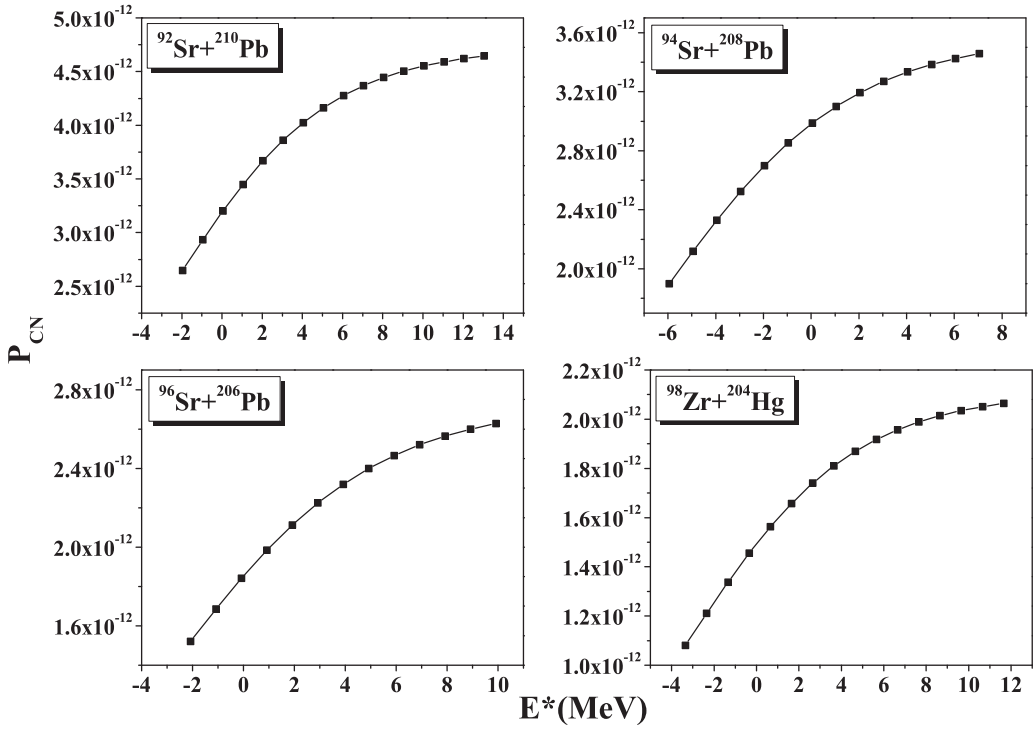

FIG. 12. The plot of P_{CN} versus E^* in MeV for the reactions of $^{92}Sr + ^{210}Pb$, $^{94}Sr + ^{208}Pb$, $^{96}Sr + ^{206}Pb$, and $^{98}Zr + ^{204}Hg$.

which is higher than in the second region $84 < A_P < 100$ where the fusion cross section is of the order of picobarns, and for the combinations in region $60 < A_P < 82$, the fusion cross section is in between that of regions I and II. The fusion cross sections for more asymmetric ("hotter") fusion reactions is found to be higher than symmetric ("colder") combinations. The combinations with large fusion cross sections are the ones which are more asymmetric and have more potential pockets (quasifission barrier).

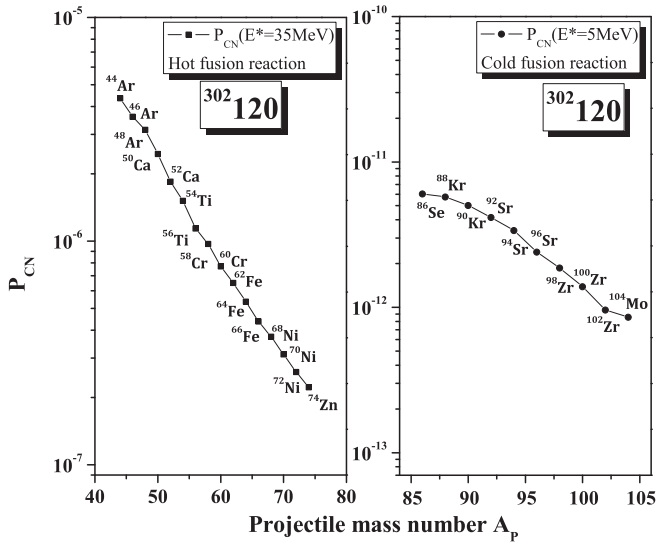

FIG. 13. Plot of P_{CN} for hot fusion ($E^* = 35$ MeV) and cold fusion ($E^* = 5$ MeV) reactions against the mass number of the projectile A_P for the SHE $^{302}120$.

For the deexcitation stage, the survival probability W_{sur} is calculated by using the formalism discussed in Sec. II B 3. We calculated the evaporation residue cross sections for the $2n$, $3n$, $4n$, and $5n$ evaporation channels for the hot combinations and the $1n$ evaporation channel for the cold combinations and plotted in the lower panels of Figs. 14–25. The predictions of the maximum value of the ER cross sections of all the probable combinations are presented in Table II. The calculated cross section for the $3n$ channel (84.21 fb) and $4n$ channel (15.67 fb) is larger for the reaction $^{48}Ca + ^{254}Fm$, and the $2n$ cross section (325.21 fb) is larger for $^{68}Ni + ^{234}U$. The predicted $1n$ cross section (shown in the lower panel of Figs. 22–25) for cold fusion combinations is too small as compared to hot fusion combinations. So to synthesize element $Z = 120$, our study reveals that the hot fusion reaction is preferable.

As shown in Figs. 14(c) and 14(d), the maximum ER cross section ($2n$ and $3n$) for $^{46}Ar + ^{256}No$ is found to be higher than $^{44}Ar + ^{258}No$. Also among the combinations $^{48}Ca + ^{254}Fm$, $^{50}Ca + ^{252}Fm$, and $^{52}Ca + ^{250}Fm$ [Figs. 15(c), 15(d), and 16(c)], our result shows that σ_{ER} is larger for $^{48}Ca + ^{254}Fm$ and is the most favorable projectile-target combination. The ER cross sections for $^{54}Ti + ^{248}Cf$ [Fig. 16(d)] are higher than $^{56}Ti + ^{246}Cf$ [Fig. 17(c)]. Among the combinations $^{58}Cr + ^{244}Cm$ [Fig. 17(d)] and $^{60}Cr + ^{242}Cm$ [Fig. 18(c)], the latter reaction is more favorable to the $2n$ channel, and the former reaction is favorable to the $3n$ and $4n$ channels. Similarly, for the reactions $^{62}Fe + ^{240}Pu$ [Fig. 18(d)], $^{64}Fe + ^{238}Pu$ [Fig. 19(c)], and $^{66}Fe + ^{236}Pu$ [Fig. 19(d)] σ_{ER} ($2n$) is more for $^{64}Fe + ^{238}Pu$, whereas σ_{ER} ($3n$ and $4n$) is more for $^{62}Fe + ^{240}Pu$. The ER cross sections of $^{68}Ni + ^{234}U$ [Fig. 20(c)] are more

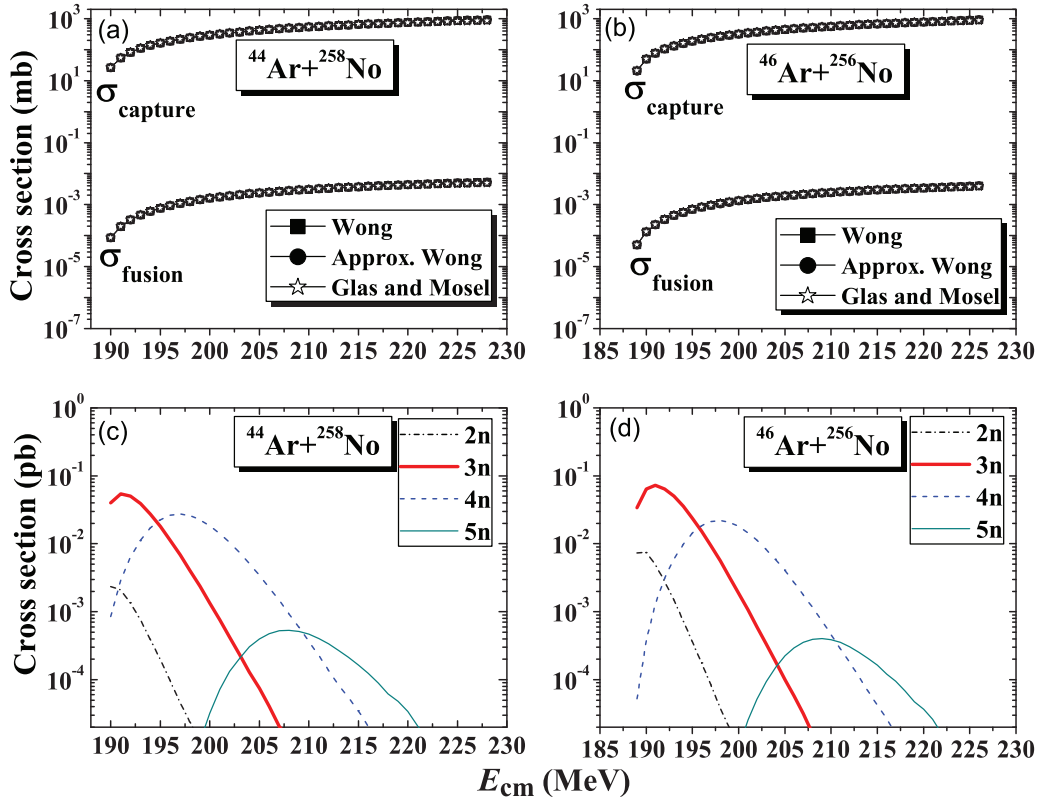

FIG. 14. Plots of capture (σ_{capture}) and fusion (σ_{fusion}) cross sections in millibarns (upper panel) and evaporation residue cross sections in picobarns (lower panel) versus center-of-mass energy E_{cm} in MeV for the reactions of $^{44}\text{Ar} + {}^{258}\text{No}$ and $^{46}\text{Ar} + {}^{256}\text{No}$.

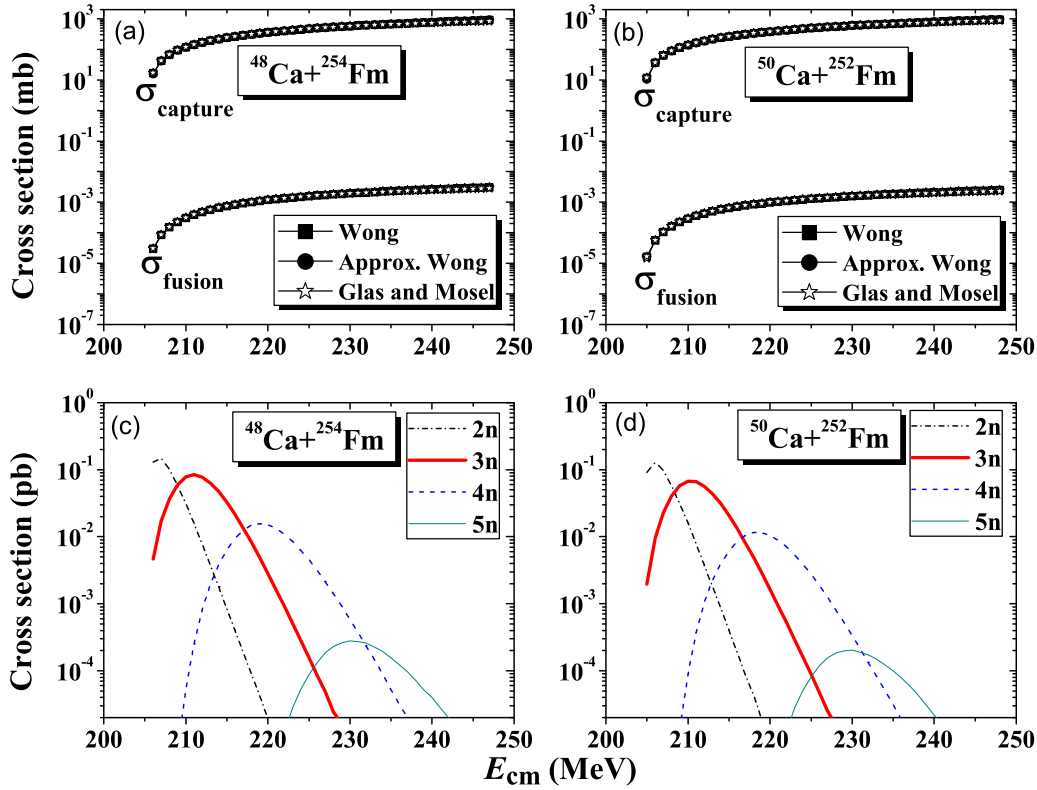

FIG. 15. Plots of capture (σ_{capture}) and fusion (σ_{fusion}) cross sections in millibarns (upper panel) and evaporation residue cross sections in picobarns (lower panel) versus center-of-mass energy E_{cm} in MeV for the reactions of $^{48}\text{Ca} + {}^{254}\text{Fm}$ and $^{50}\text{Ca} + {}^{252}\text{Fm}$.

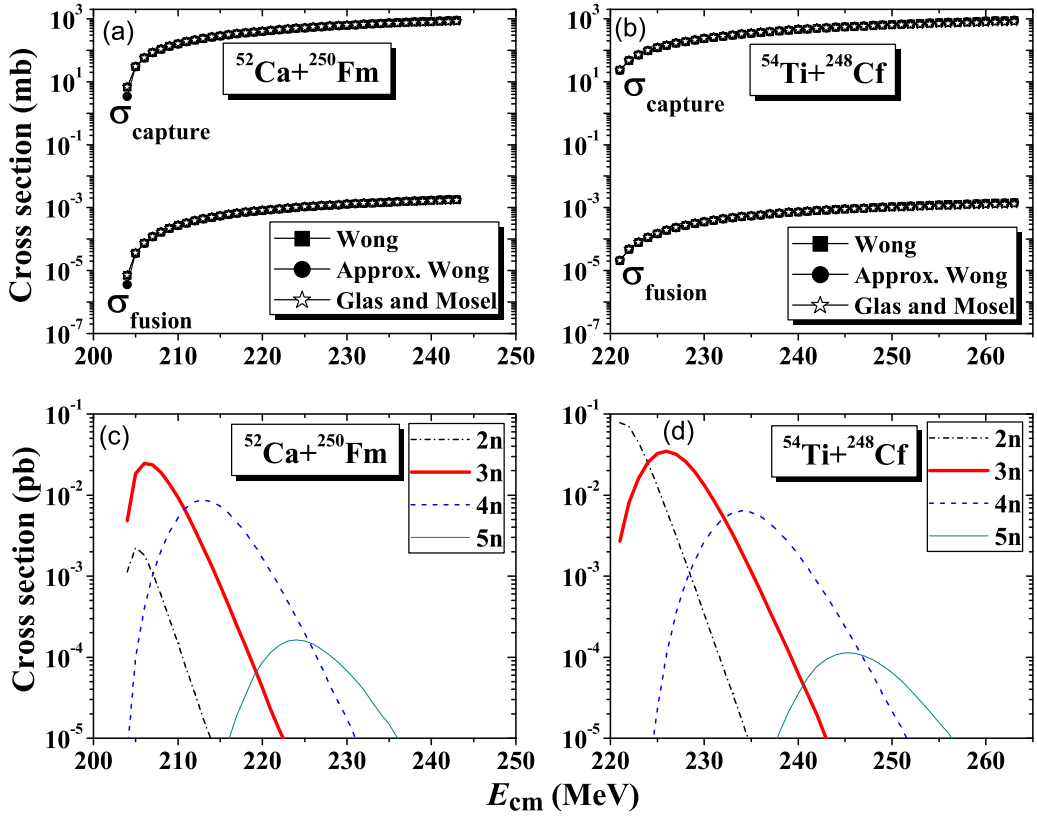

FIG. 16. Plots of capture ($\sigma_{capture}$) and fusion (σ_{fusion}) cross sections in millibarns (upper panel) and evaporation residue cross sections in picobarns (lower panel) versus center-of-mass energy E_{cm} in MeV for the reactions of ^{52}Ca + ^{250}Fm and ^{54}Ti + ^{248}Cf.

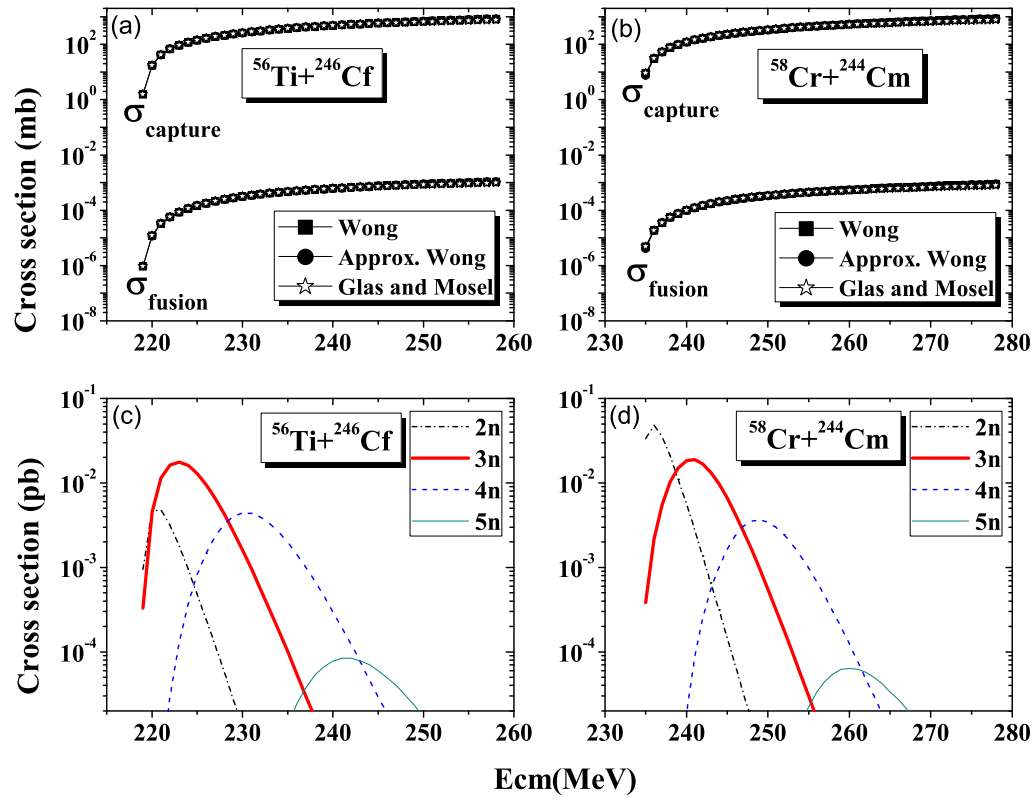

FIG. 17. Plots of capture ($\sigma_{capture}$) and fusion (σ_{fusion}) cross sections in millibarns (upper panel) and evaporation residue cross sections in picobarns (lower panel) versus center-of-mass energy E_{cm} in MeV for the reactions of ^{56}Ti + ^{246}Cf and ^{58}Cr + ^{244}Cm.

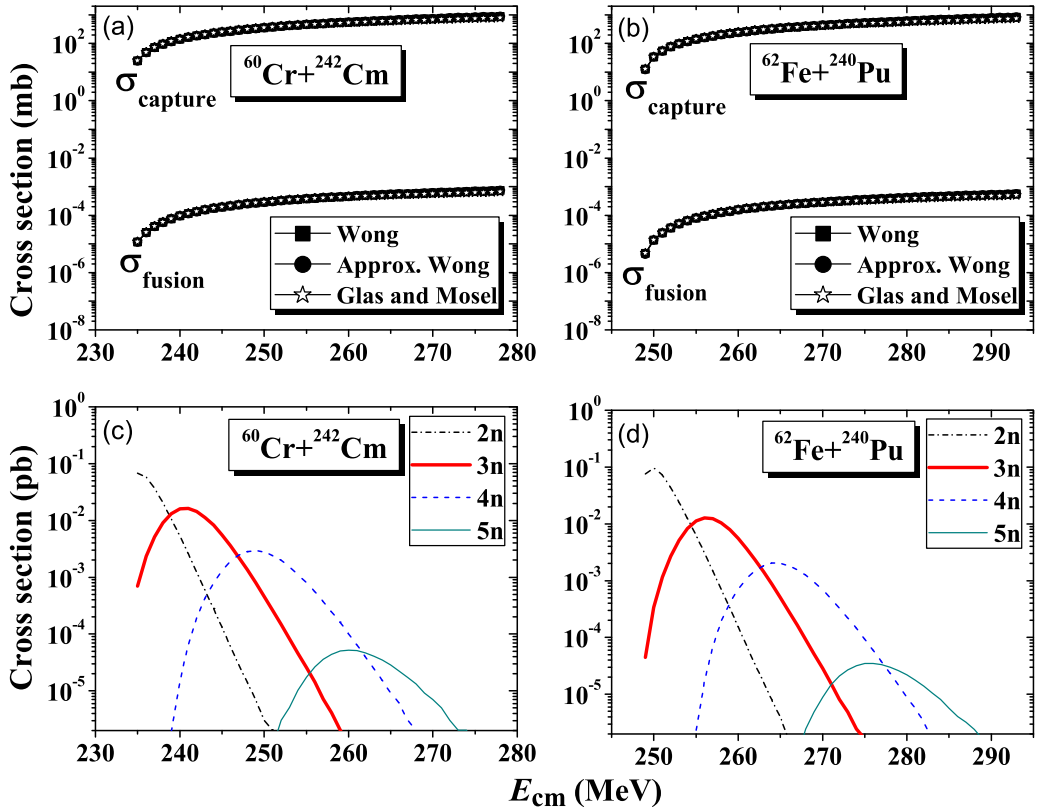

FIG. 18. Plots of capture (σ_{capture}) and fusion (σ_{fusion}) cross sections in millibarns (upper panel) and evaporation residue cross sections in picobarns (lower panel) versus center-of-mass energy E_{cm} in MeV for the reactions of $^{60}\text{Cr} + ^{242}\text{Cm}$ and $^{62}\text{Fe} + ^{240}\text{Pu}$.

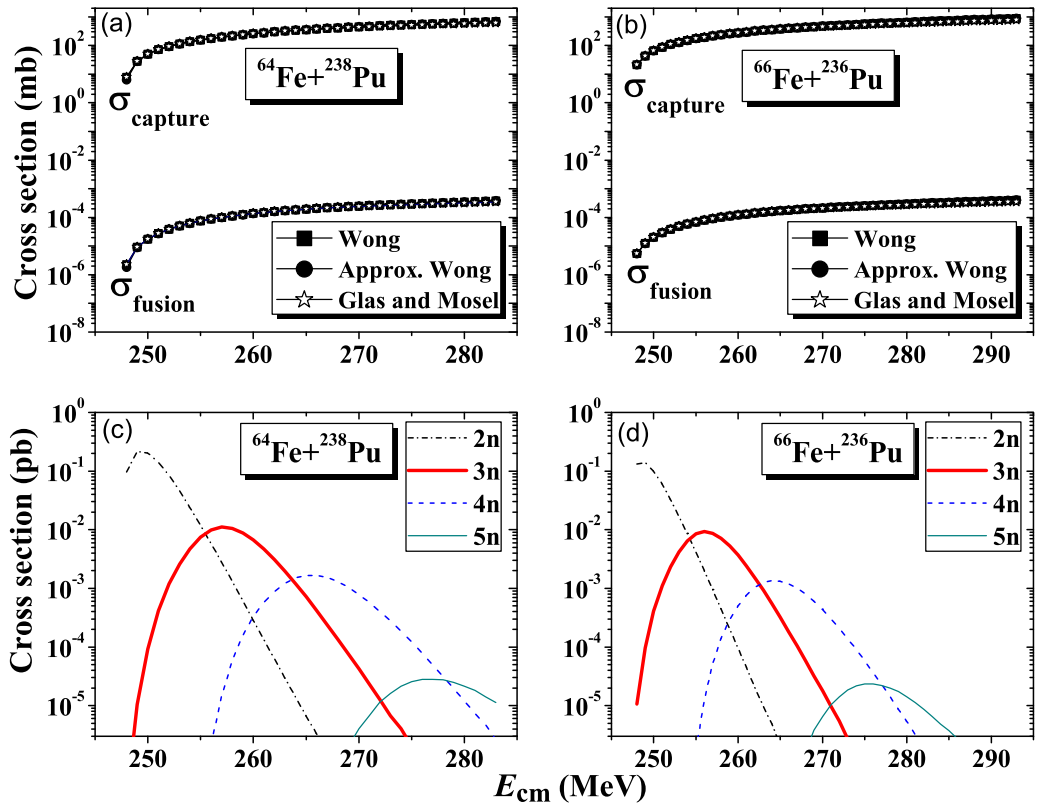

FIG. 19. Plots of capture (σ_{capture}) and fusion (σ_{fusion}) cross sections in millibarns (upper panel) and evaporation residue cross sections in picobarns (lower panel) versus center-of-mass energy E_{cm} in MeV for the reactions of $^{64}\text{Fe} + ^{238}\text{Pu}$ and $^{66}\text{Fe} + ^{236}\text{Pu}$.

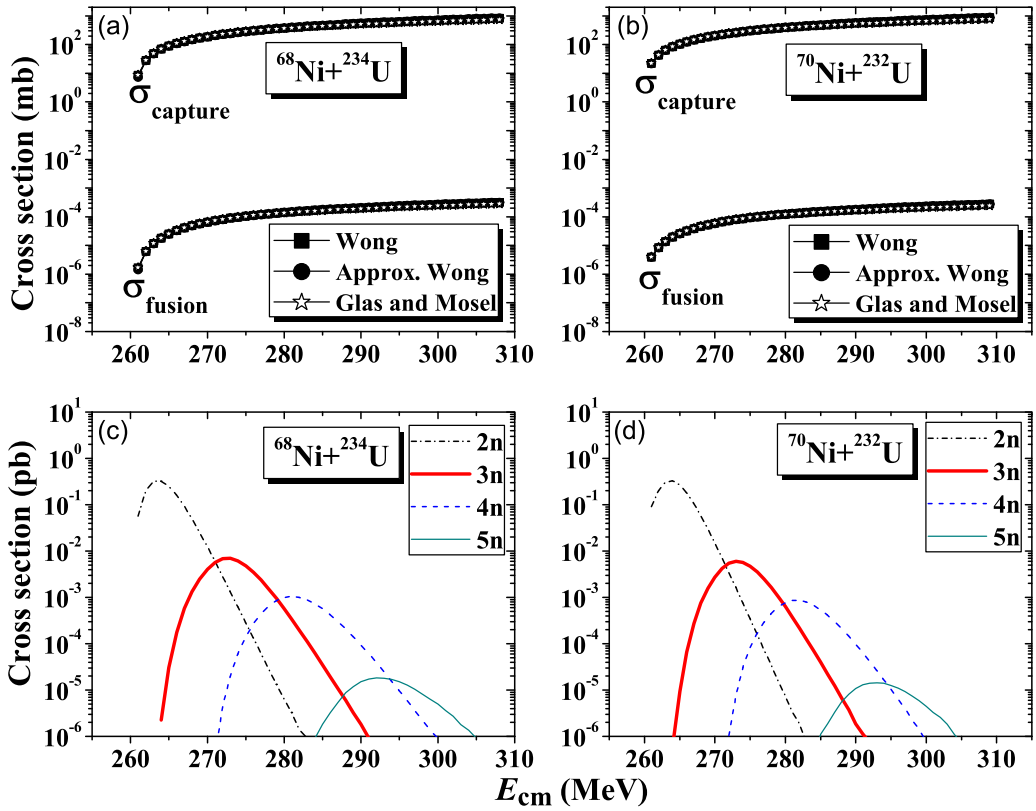

FIG. 20. Plots of capture ($\sigma_{capture}$) and fusion (σ_{fusion}) cross sections in millibarns (upper panel) and evaporation residue cross sections in picobarns (lower panel) versus center-of-mass energy E_{cm} in MeV for the reactions of ^{68}Ni + ^{234}U and ^{70}Ni + ^{232}U.

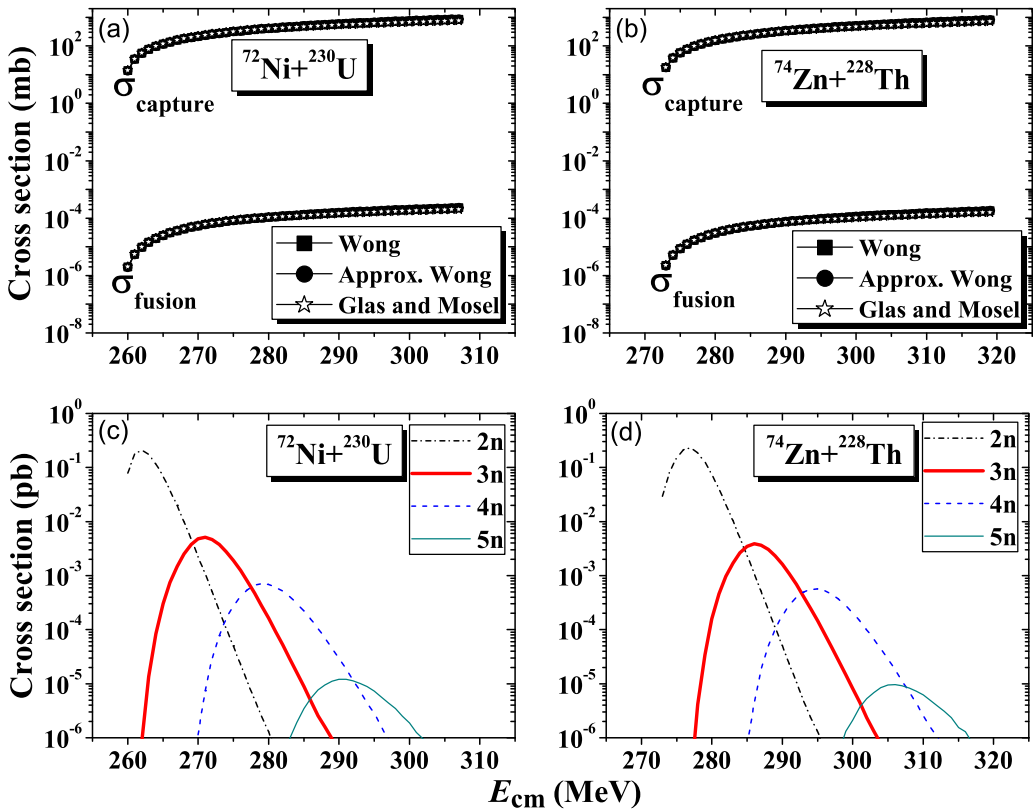

FIG. 21. Plots of capture ($\sigma_{capture}$) and fusion (σ_{fusion}) cross sections in millibarns (upper panel) and evaporation residue cross sections in picobarns (lower panel) versus center-of-mass energy E_{cm} in MeV for the reactions of ^{72}Ni + ^{230}U and ^{74}Zn + ^{228}Th.

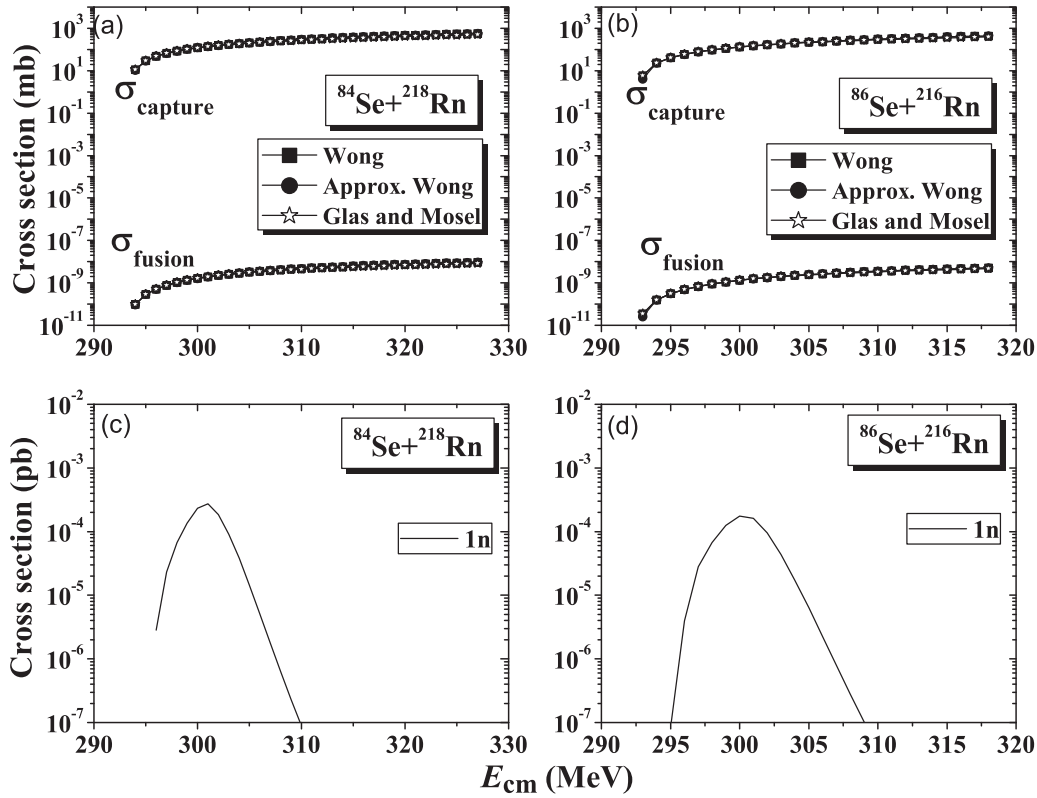

FIG. 22. Plots of capture (σ_{capture}) and fusion (σ_{fusion}) cross sections in millibarns (upper panel) and evaporation residue cross sections in picobarns (lower panel) versus center-of-mass energy E_{cm} in MeV for the reactions of $^{84}\text{Se} + ^{218}\text{Rn}$ and $^{86}\text{Se} + ^{216}\text{Rn}$.

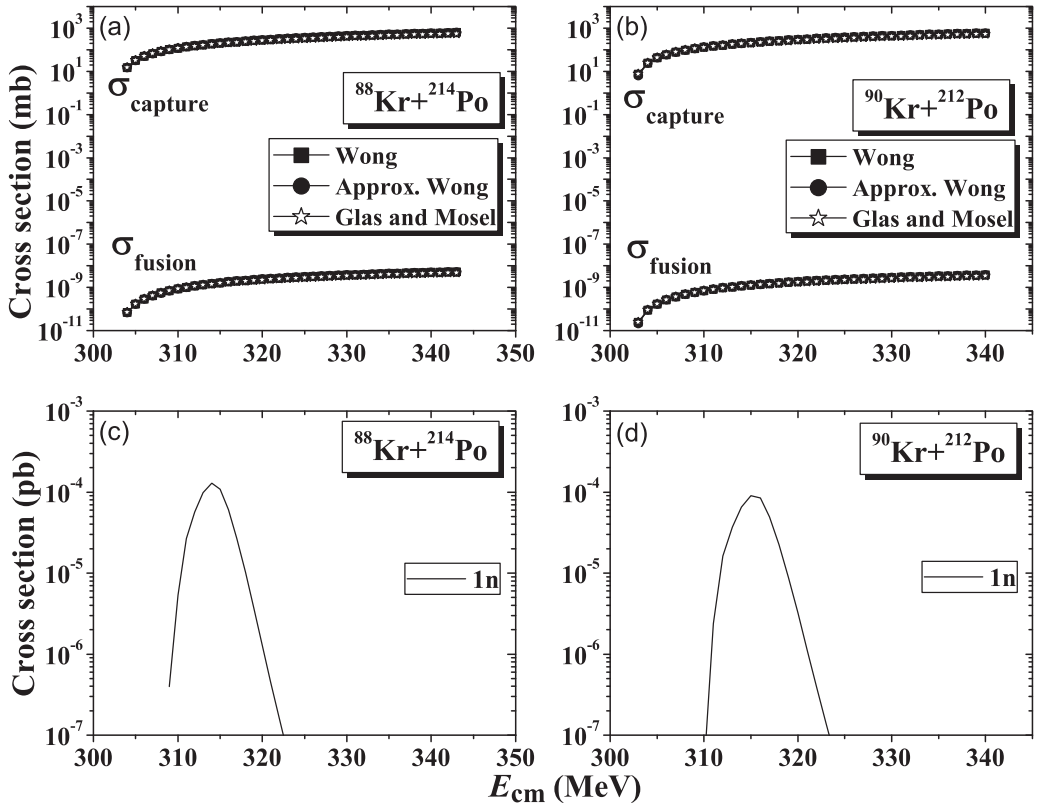

FIG. 23. Plots of capture (σ_{capture}) and fusion (σ_{fusion}) cross sections in millibarns (upper panel) and evaporation residue cross sections in picobarns (lower panel) versus center-of-mass energy E_{cm} in MeV for the reactions of $^{88}\text{Kr} + ^{214}\text{Po}$ and $^{90}\text{Kr} + ^{212}\text{Po}$.

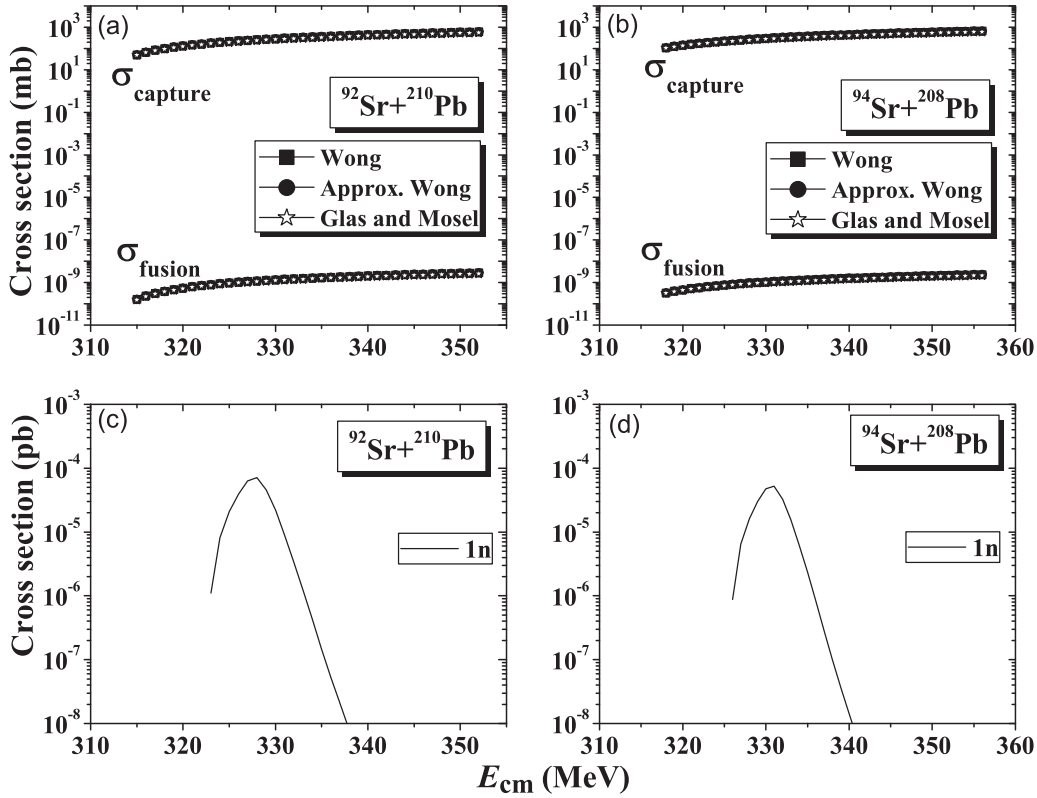

FIG. 24. Plots of capture (σ_{capture}) and fusion (σ_{fusion}) cross sections in millibarns (upper panel) and evaporation residue cross sections in picobarns (lower panel) versus center-of-mass energy E_{cm} in MeV for the reactions of $^{92}\text{Sr} + {}^{210}\text{Pb}$ and $^{94}\text{Sr} + {}^{208}\text{Pb}$.

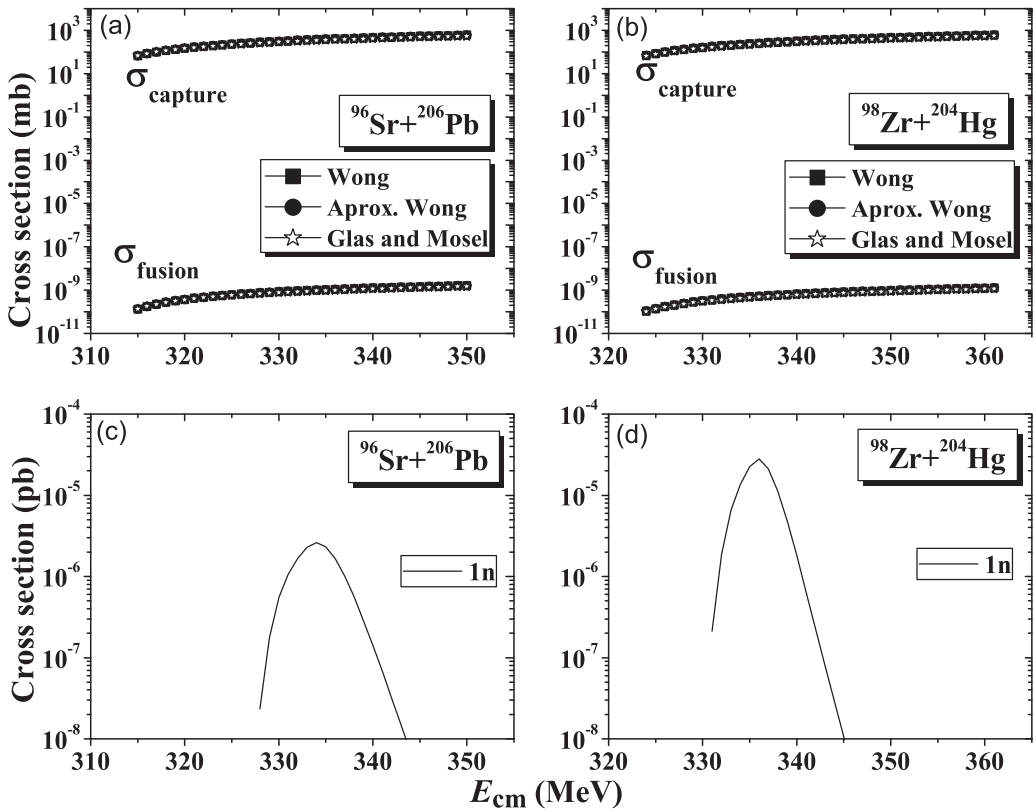

FIG. 25. Plots of capture (σ_{capture}) and fusion (σ_{fusion}) cross sections in millibarns (upper panel) and evaporation residue cross sections in picobarns (lower panel) versus center-of-mass energy E_{cm} in MeV for the reactions of $^{96}\text{Sr} + {}^{206}\text{Pb}$ and $^{98}\text{Zr} + {}^{204}\text{Hg}$.

TABLE II. Calculated maximum values of the evaporation residue cross sections for the probable hot and cold fusion combinations found in the cold valley of $^{302}120$.

Combinations for hot fusion reactions	$\sigma_{ER}(2n)$ (fb)	$\sigma_{ER}(3n)$ (fb)	$\sigma_{ER}(4n)$ (fb)	$\sigma_{ER}(5n)$ (fb)	Combinations for cold fusion reactions	$\sigma_{ER}(1n)$ (fb)
$^{44}Ar+^{258}No$	2.3513	54.210	27.393	0.5343	$^{84}Se+^{218}Rn$	0.2740
$^{46}Ar+^{256}No$	7.4563	72.232	22.063	0.4020	$^{86}Se+^{216}Rn$	0.1753
$^{48}Ca+^{254}Fm$	146.89	84.207	15.669	0.2776	$^{88}Kr+^{214}Po$	0.1283
$^{50}Ca+^{252}Fm$	130.83	67.579	11.536	0.2020	$^{90}Kr+^{212}Po$	0.0906
$^{52}Ca+^{250}Fm$	2.2783	24.631	8.7108	0.1629	$^{92}Sr+^{210}Pb$	0.0715
$^{54}Ti+^{248}Cf$	78.024	34.790	6.4196	0.1116	$^{94}Sr+^{208}Pb$	0.0523
$^{56}Ti+^{246}Cf$	4.7816	17.639	4.4012	0.0844	$^{96}Sr+^{206}Pb$	0.0406
$^{58}Cr+^{244}Cm$	48.458	18.865	3.6606	0.0638	$^{98}Zr+^{204}Hg$	0.0281
$^{60}Cr+^{242}Cm$	67.820	16.252	2.9514	0.0521		
$^{62}Fe+^{240}Pu$	96.964	12.805	2.0295	0.0350		
$^{64}Fe+^{238}Pu$	215.07	11.067	1.6679	0.0282		
$^{66}Fe+^{236}Pu$	139.08	9.2581	1.3610	0.0233		
$^{68}Ni+^{234}U$	325.21	6.9364	1.0514	0.0183		
$^{70}Ni+^{232}U$	303.75	6.0200	0.8626	0.0144		
$^{72}Ni+^{230}U$	209.49	5.1034	0.7114	0.0121		
$^{74}Zn+^{228}Th$	228.78	3.8634	0.5699	0.0097		
$^{54}Cr+^{248}Cm$[a]	1.3288	15.398	5.0357	0.0950		
$^{58}Fe+^{244}Pu$[a]	0.4329	6.1166	2.7777	0.0580		
$^{64}Ni+^{238}U$[a]	11.250	7.8063	1.4923	0.0267		
$^{50}Ti+^{249}Cf$[a]	0.4140	102.92	2.2642	0.3784		

[a]Combinations for which experimental studies were performed.

than $^{70}Ni+^{232}U$ [Fig. 20(d)] and $^{72}Ni+^{230}U$ [Fig. 21(c)] systems. Based on the arguments of the quasifission barrier, reaction asymmetry, excitation energy, the probability of compound nucleus formation, and survival probability, the most promising choices for an attempt to synthesize element $^{302}120$ are $^{44}Ar+^{258}No$, $^{46}Ar+^{256}No$, $^{48}Ca+^{254}Fm$,

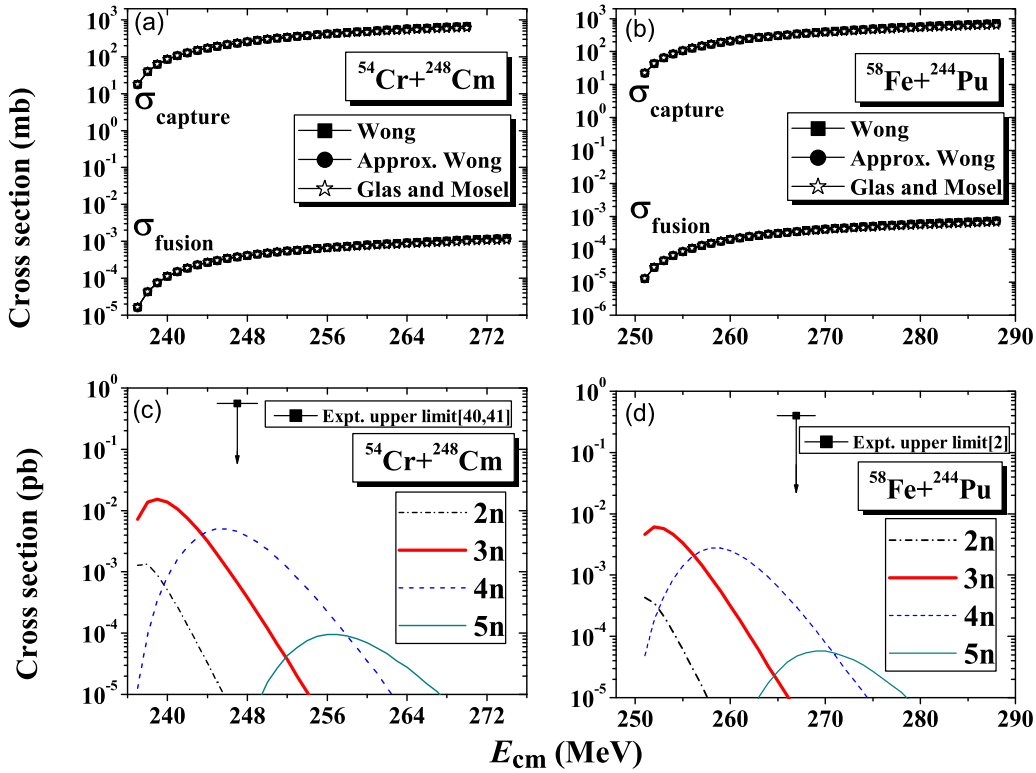

FIG. 26. Plots of capture ($\sigma_{capture}$) and fusion (σ_{fusion}) cross sections in millibarns (upper panel) and evaporation residue cross sections in picobarns (lower panel) versus center-of-mass energy E_{cm} in MeV for the reactions of $^{54}Cr+^{248}Cm$ and $^{58}Fe+^{244}Pu$.

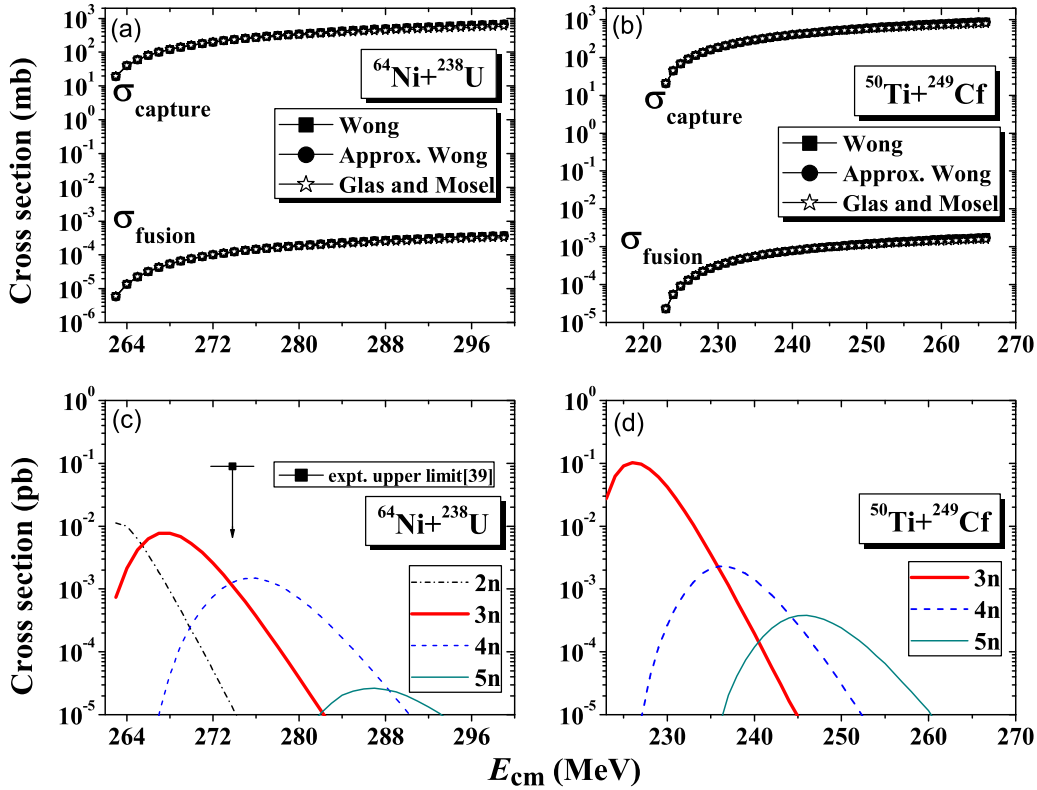

FIG. 27. Plots of capture ($\sigma_{capture}$) and fusion (σ_{fusion}) cross sections in millibarns (upper panel) and evaporation residue cross sections in picobarns (lower panel) versus center-of-mass energy E_{cm} in MeV for the reactions of ^{64}Ni + ^{238}U and ^{50}Ti + ^{249}Cf.

^{50}Ca + ^{252}Fm, ^{54}Ti + ^{248}Cf, ^{58}Cr + ^{244}Cm, ^{62}Fe + ^{240}Pu, ^{64}Fe + ^{238}Pu, ^{68}Ni + ^{234}U, ^{70}Ni + ^{232}U, ^{72}Ni + ^{230}U, and ^{74}Zn + ^{228}Th.

In order to check the consistency of our calculations, we have evaluated the capture, fusion, and evaporation residue cross sections of four reactions, ^{54}Cr + ^{248}Cm, ^{58}Fe + ^{244}Pu, ^{64}Ni + ^{238}U, and ^{50}Ti + ^{249}Cf for which several theoretical studies and the attempt to produce the element $Z = 120$ were performed. Figure 26 shows the predicted capture, fusion, and ER cross sections for ^{54}Cr + ^{248}Cm and ^{58}Fe + ^{244}Pu systems. The calculated $3n$ and $4n$ channel ER cross sections for the reaction ^{54}Cr + ^{248}Cm [Fig. 26(c)] are 15.4 and 5.04 fb, respectively, and for the ^{58}Fe + ^{244}Pu reaction [Fig. 26(d)], they are found to be 6.12 and 2.78 fb, respectively. The excitation functions for ^{64}Ni + ^{238}U and ^{50}Ti + ^{249}Cf are shown in Fig. 27. The $3n$ and $4n$ channel maximum ER cross sections for ^{64}Ni + ^{238}U [Fig. 27(c)] are 7.81 and 1.49 fb, respectively, and that of ^{50}Ti + ^{249}Cf [Fig. 27(d)] are 102.92 and 2.264 fb, respectively. We have observed that the more mass asymmetric ^{50}Ti + ^{249}Cf is more favorable to synthesize element $Z = 120$ because $3n$ and $4n$ evaporation residue cross sections are much larger than the maximal values for the other reactions. To compare the results with other models, we listed the maximum ER cross sections ($3n$ and $4n$) for the combinations ^{54}Cr + ^{248}Cm, ^{58}Fe + ^{244}Pu, ^{64}Ni + ^{238}U, and ^{50}Ti + ^{249}Cf in Tables III and IV. The calculated maximum $3n$ and $4n$ evaporation residue cross sections for the above-mentioned combinations are of the same order with other

TABLE III. Comparison of predicted maximum values of the evaporation residue cross sections [$\sigma_{ER}(3n)$ and $\sigma_{ER}(4n)$] for ^{54}Cr + ^{248}Cm and ^{58}Fe + ^{244}Pu with our results. The maximum values of the presented data were taken from the figures of the ER excitation functions of the given references.

^{54}Cr + ^{248}Cm				^{58}Fe + ^{244}Pu				Reference
E_{cm} (MeV)	$\sigma_{ER}(3n)$ (fb)	E_{cm} (MeV)	$\sigma_{ER}(4n)$ (fb)	E_{cm} (MeV)	$\sigma_{ER}(3n)$ (fb)	E_{cm} (MeV)	$\sigma_{ER}(4n)$ (fb)	
246.0	14.0	250.0	28.0	264.0	2.0	265.0	5.0	[44]
240.5	0.7	249.0	0.4					[52]
237.2	55.0	241.0	13.0					[49]
241.0	160	252.0	12.0	255.0	12.0	265.0	1.8	[34]
238.0	2.0	250.0	5.0	252.0	0.9	263.0	2.2	[50]
240.0	0.6	250.0	3.0					[54]
239.0	15.4	245.0	5.04	252.0	6.12	258.0	2.78	This work

TABLE IV. Comparison of predicted maximum values of the evaporation residue cross sections [$\sigma_{ER}(3n)$ and $\sigma_{ER}(4n)$] for $^{64}Ni + ^{238}U$ and $^{50}Ti + ^{249}Cf$ with our results. The maximum values of the presented data were taken from the figures of the ER excitation functions of the given references.

$^{64}Ni + ^{238}U$				$^{50}Ti + ^{249}Cf$				Reference
E_{cm} (MeV)	$\sigma_{ER}(3n)$ (fb)	E_{cm} (MeV)	$\sigma_{ER}(4n)$ (fb)	E_{cm} (MeV)	$\sigma_{ER}(3n)$ (fb)	E_{cm} (MeV)	$\sigma_{ER}(4n)$ (fb)	
273.0	4.5	277.0	3.0	236.0	40	241	46	[44]
				240.5	5.5	249	6.1	[52]
				225.0	100	231.5	2.5	[49]
273.0	7.0	283.0	1.0	227.5	760	239	28	[34]
				227.0	20	240	4.5	[50]
				229.0	20	240	21	[54]
				231.5	60	232.5	40	[80]
				230.0	150	239	50	[53]
				230.0	50	245	3.5	[51]
268.0	7.81	276.0	1.49	226.0	102.92	237	2.264	This work

theoretical models, and $^{50}Ti + ^{249}Cf$ is found to be the more feasible combination in all the theoretical studies, which very well establishes the reliability of our paper. Note that the experimental upper limit for the above reactions $^{58}Fe + ^{244}Pu$, $^{64}Ni + ^{238}U$, and $^{54}Cr + ^{248}Cm$ had been established at 400 fb [2], 90 fb [39], 560 fb [40,41], respectively, and an attempt was performed using the reactions $^{50}Ti + ^{249}Cf$ [85]. Recently Hofmann *et al.* [86] measured the cross section for the three event chains observed in the reaction $^{54}Cr + ^{248}Cm$ tentatively assigned to $^{299}120$ is $0.58^{+1.34}_{-0.48}$ pb.

IV. CONCLUSIONS

Probable target-projectile combinations for the superheavy element $^{302}120$ have been identified from the cold reaction valleys. We have calculated the interaction barriers for fusion of all the projectile-target combinations identified in the cold valleys of the superheavy $^{302}120$ nucleus, against the distance between the centers of the projectile and the target by taking the Coulomb and proximity potential as the scattering potential. Near and above the barrier, the total capture, fusion, and ER cross sections for all the systems also have been calculated. The systems $^{44}Ar + ^{258}No$, $^{46}Ar + ^{256}No$, $^{48}Ca + ^{254}Fm$, $^{50}Ca + ^{252}Fm$, $^{52}Ca + ^{250}Fm$, $^{54}Ti + ^{248}Cf$, $^{56}Ti + ^{246}Cf$, and $^{58}Cr + ^{244}Cm$ in deep region I of the cold valley and the systems $^{60}Cr + ^{242}Cm$, $^{62}Fe + ^{240}Pu$, $^{64}Fe + ^{238}Pu$, $^{66}Fe + ^{236}Pu$, $^{68}Ni + ^{234}U$, $^{70}Ni + ^{232}U$, $^{72}Ni + ^{230}U$, and $^{74}Zn + ^{228}Th$ in the cold valleys are identified as the better projectile-target combinations for the synthesis of $^{302}120$. While considering the nature of the quasifission barrier height and half-lives of the colliding nuclei, mass asymmetry, the probability of compound nucleus formation, survival probability, and excitation energy, the systems $^{44}Ar + ^{258}No$, $^{46}Ar + ^{256}No$, $^{48}Ca + ^{254}Fm$, $^{50}Ca + ^{252}Fm$, $^{54}Ti + ^{248}Cf$, $^{58}Cr + ^{244}Cm$, $^{62}Fe + ^{240}Pu$, $^{64}Fe + ^{238}Pu$, $^{68}Ni + ^{234}U$, $^{70}Ni + ^{232}U$, $^{72}Ni + ^{230}U$, and $^{74}Zn + ^{228}Th$ give the maximum probability for the synthesis of the superheavy nucleus $^{302}120$. The computed ER cross sections for $^{54}Cr + ^{248}Cm$, $^{58}Fe + ^{244}Pu$, $^{64}Ni + ^{238}U$, and $^{50}Ti + ^{249}Cf$ combinations are compared with experimental data and other theoretical models, and all models predicted the maximum cross section for the combination $^{50}Ti + ^{249}Cf$, which proves the reliability of our work. Through our extensive study, we predict several promising possibilities for the synthesis of the SHE $^{302}120$.

ACKNOWLEDGMENTS

One of the authors (VS) would like to thank the University Grants Commission (UGC), Government of India for the financial support in the form of Moulana Azad National Fellowship (MANF).

[1] J. H. Hamilton, S. Hofmann, and Y. T. Oganessian, Annu. Rev. Nucl. Part. Sci. **63**, 383 (2013).
[2] Y. T. Oganessian, V. K. Utyonkov, Y. V. Lobanov, F. S. Abdullin, A. N. Polyakov, R. N. Sagaidak, I. V. Shirokovsky, Y. S. Tsyganov, A. A. Voinov, A. N. Mezentsev, V. G. Subbotin, A. M. Sukhov, K. Subotic, V. I. Zagrebaev, and S. N. Dmitriev, Phys. Rev. C **79**, 024603 (2009).
[3] B. B. Back, H. Esbensen, C. L. Jiang, and K. E. Rehm, Rev. Mod. Phys. **86**, 317 (2014).
[4] S. Hofmann and G. Munzenberg, Rev. Mod. Phys. **72**, 733 (2000).
[5] S. Hofmann, F. P. Heßberger, D. Ackermann, G. Münzenberg, S. Antalic, P. Cagarda, B. Kindler, J. Kojouharova, M. Leino, B. Lommel, R. Mann, A. G. Popeko, S. Reshitko, S. Saro, J. Uusitalo, and A. V. Yeremin, Eur. Phys. J. A **14**, 147 (2002).
[6] K. Morita, K. Morimoto, D. Kaji, T Akiyama, S. Goto, H. Haba, E. Ideguchi, K. Katori, H. Koura, H. Kudo, T. Ohnishi, A. Ozawa, T. Suda, K. Sueki, F. Tokanai, T. Yamaguchi, A. Yoneda, and A. Yoshida, J. Phys. Soc. Jpn. **76**, 043201 (2007).
[7] Y. T. Oganessian, V. K. Utyonkov, Y. V. Lobanov, F. S. Abdullin, A. N. Polyakov, R. N. Sagaidak, I. V. Shirokovsky, Y. S. Tsyganov, A. A. Voinov, G. G. Gulbekian, S. L. Bogomolov,

B. N. Gikal, A. N. Mezentsev, S. Iliev, V. G. Subbotin, A. M. Sukhov, K. Subotic, V. I. Zagrebaev, G. K. Vostokin, M. G. Itkis, K. J. Moody, J. B. Patin, D. A. Shaughnessy, M. A. Stoyer, N. J. Stoyer, P. A. Wilk, J. M. Kenneally, J. H. Landrum, J. F. Wild, and R. W. Lougheed, Phys. Rev. C **74**, 044602 (2006).

[8] Y. T. Oganessian, F. S. Abdullin, P. D. Bailey, D. E. Benker, M. E. Bennett, S. N. Dmitriev, J. G. Ezold, J. H. Hamilton, R. A. Henderson, M. G. Itkis, Y. V. Lobanov, A. N. Mezentsev, K. J. Moody, S. L. Nelson, A. N. Polyakov, C. E. Porter, A. V. Ramayya, F. D. Riley, J. B. Roberto, M. A. Ryabinin, K. P. Rykaczewski, R. N. Sagaidak, D. A. Shaughnessy, I. V. Shirokovsky, M. A. Stoyer, V. G. Subbotin, R. Sudowe, A. M. Sukhov, R. Taylor, Y. S. Tsyganov, V. K. Utyonkov, A. A. Voinov, G. K. Vostokin, and P. A. Wilk, Phys. Rev. C **83**, 054315 (2011).

[9] Y. T. Oganessian, F. S. Abdullin, S. N. Dmitriev, J. M. Gostic, J. H. Hamilton, R. A. Henderson, M. G. Itkis, K. J. Moody, A. N. Polyakov, A. V. Ramayya, J. B. Roberto, K. P. Rykaczewski, R. N. Sagaidak, D. A. Shaughnessy, I. V. Shirokovsky, M. A. Stoyer, N. J. Stoyer, V. G. Subbotin, A. M. Sukhov, Y. S. Tsyganov, V. K. Utyonkov, A. A. Voinov, and G. K. Vostokin, Phys. Rev. C **87**, 014302 (2013).

[10] Y. T. Oganessian and V. K. Utyonkov, Rep. Prog. Phys. **78**, 036301 (2015).

[11] V. K. Utyonkov, N. T. Brewer, Y. T. Oganessian, K. P. Rykaczewski, F. S. Abdullin, S. N. Dmitriev, R. K. Grzywacz, M. G. Itkis, K. Miernik, A. N. Polyakov, J. B. Roberto, R. N. Sagaidak, I. V. Shirokovsky, M. V. Shumeiko, Y. S. Tsyganov, A. A. Voinov, V. G. Subbotin, A. M. Sukhov, A. V. Sabel'nikov, G. K. Vostokin, J. H. Hamilton, M. A. Stoyer, and S. Y. Strauss, Phys. Rev. C **92**, 034609 (2015).

[12] V. I. Zagrebaev, A. V. Karpov, and W. Greiner, Phys. Rev. C **85**, 014608 (2012).

[13] N. Wang, E. G. Zhao, and W. Scheid, Phys. Rev. C **89**, 037601 (2014).

[14] T. Banergee, S. Nath, and S. Pal, Phys. Rev. C **91**, 034619 (2015).

[15] K. Hagino, N. Rowley, and A. T. Kruppa, Comput. Phys. Commun. **123**, 143 (1999).

[16] Z. H. Liu and J. D. Bao, Phys. Rev. C **83**, 044613 (2011).

[17] Y. Abe, B. Bouriguet, G. Kosenko, and C. Shen, Nucl. Phy. A **734**, 168 (2004).

[18] C. Shen, G. Kosenko, and Y. Abe, Phys. Rev. C **66**, 061602(R) (2002).

[19] V. I. Zagrebaev, Phys. Rev. C **64**, 034606 (2001).

[20] V. I. Zagrebaev, *Tours Symposium on Nuclear Physics V*, edited by M. Arnould, M. Lewitowicz, G. Münzenberg, H. Akimune, M. Ohta, H. Utsunomiya, T. Wada, and T. Yamagata, AIP Conf. Proc. No. 704 (AIP, New York, 2004), p. 31.

[21] G. Adamian, N. Antonenko, and W. Scheid, Nucl. Phys. A **618**, 176 (1997).

[22] Z. Q. Feng, G.-M. Jin, F. Fu, and J. Q. Li, Nucl. Phys. A **771**, 50 (2006).

[23] M. Huang, Z. Gan, X. Zhou, J. Li, and W. Scheid, Phys. Rev. C **82**, 044614 (2010).

[24] V. V. Volkov, N. A. Antonenko, E. A. Cherepanov, A. K. Nasirov, and V. P. Permjakov, Phys. Lett. B **319**, 425 (1993).

[25] A. Nasirov, K. Kim, G. Mandaglio, G. Giardina, A. Muminov, and Y. Kim, Eur. Phys. J. A **49**, 147 (2013).

[26] W. Li, N. Wang, F. Jia, H. Xu, W. Zuo, Q. Li, E. Zhao, J. Li, and W. Scheid, J. Phys. G: Nucl. Phys. **32**, 1143 (2006).

[27] K. P. Santhosh and B. Priyanka, J. Phys. G: Nucl. Part. Phys. **39**, 085106 (2012).

[28] K. P. Santhosh and B. Priyanka, Phys. Rev. C **87**, 064611 (2013).

[29] K. P. Santhosh and B. Priyanka, Phys. Rev. C **89**, 064604 (2014).

[30] A. Sobiczewski, F. A. Gareev, and B. N. Kalinkin, Phys. Lett. **22**, 500 (1966).

[31] H. Meldner, Ark. Fys. **36**, 593 (1967).

[32] W. D. Myer and W. J. Swiatecki, Nucl. Phys. A **81**, 1 (1996).

[33] M. A. Stoyer, Nature (London) **442**, 876 (2006).

[34] K. Siwek-Wilczyńska, T. Cap, and J. Wilczyński, Int. J. Mod. Phys. E **19**, 500 (2010).

[35] G. G. Adamian, N. V. Antonenko, W. Scheid, and V. V. Volkov, Nucl. Phys. A **633**, 409 (1998).

[36] N. Wang and M. Liu, Nucl. Phys. A **834**, 212 (2010).

[37] R. Bock, Y. T. Chu, M. Dakowski, A. Gobbi, E. Grosse, A. Olmi, H. Sann, D. Schwalm, U. Lynen, W. Müller, S. Bjørnholm, H. Esbensen, W. Wölfli, and E. Morenzoni, Nucl. Phys. A **388**, 334 (1982).

[38] E. A Cherepanov, Nucl. Phys. A **734**, E13 (2004).

[39] S. Hofmann *et al.*, GSI Scientific reports, 2008, p. 131.

[40] S. Hofmann *et al.*, GSI Scientific reports, 2011, p. 205.

[41] S. Heinz, EPJ Web Conf. **38**, 01002 (2012).

[42] E. M. Kozulin, G. N. Knyazheva, I. M. Itkis, M. G. Itkis, A. A. Bogachev, L. Krupa, T. A. Loktev, S. V. Smirnov, V. I. Zagrebaev, J. Äystö, W. H. Trzaska, V. A. Rubchenya, E. Vardaci, A. M. Stefanini, M. Cinauseroc, L. Corradi, E. Fioretto, P. Mason, G. F. Prete, R. Silvestri, S. Beghini, G. Montagnoli, F. Scarlassara, F. Hanappe, S. V. Khlebnikov, J. Kliman, A. Brondi, A. Di Nitto, R. Moro, N. Gelli, and S. Szilner, Phys. Lett. B **686**, 227 (2010).

[43] W. Loveland, Phys. Rev. C **76**, 014612 (2007).

[44] V. Zagrebaev and W. Greiner, Phys. Rev. C **78**, 034610 (2008).

[45] Z. H. Liu and J. Dong Bao, Phys. Rev. C **80**, 054608 (2009).

[46] G. G. Adamian, N. V. Antonenko, and W. Schied, Eur. Phys. J. A **41**, 235 (2009).

[47] A. K. Nasirov, G. Giardina, G. Mandaglio, M. Manganaro, F. Hanappe, S. Heinz and S. Hofmann, A. I. Muminov, and W. Scheid, Phys. Rev. C **79**, 024606 (2009).

[48] G. Giardina, G. Fazio, G. Mandaglio, M. Manganaro, A. K. Nasirov, M. Romaniuk, and C. Sacca, Int. J. Mod. Phys. E **19**, 882 (2010).

[49] A. K. Nasirov, G. Mandaglio, G. Giardina, A. Sobiczewski, and A. I. Muminov, Phys. Rev. C **84**, 044612 (2011).

[50] N. Wang, J. Tian, and W. Scheid, Phys. Rev. C **84**, 061601 (2011).

[51] N. Wang, E. G. Zhao, W. Scheid, and S.-G. Zhou, Phys. Rev. C **85**, 041601(R) (2012).

[52] K. Siwek-Wilczyńska, T. Cap, M. Kowal, A. Sobiczewski, and J. Wilzyński, Phys. Rev. C **86**, 014611 (2012).

[53] J. Zhang, C. Wang, and Z. Ren, Nucl. Phys. A **909**, 36 (2013).

[54] L. Zhu, W. J. Xie, and F. S. Zhang, Phys. Rev. C **89**, 024615 (2014).

[55] X. J. Bao, Y. Gao, J. Q. Li, and H. F. Zhang, Phys. Rev. C **91**, 011603 (2015).

[56] W. Loveland, Eur. Phys. J. A **51**, 120 (2015).

[57] K. P. Santhosh, V. Bobby Jose, A. Joseph, and K. M. Varier, Nucl. Phys. A **817**, 35 (2009).

[58] K. P. Santhosh and V. Bobby Jose, Nucl. Phys. A **922**, 191 (2014).

[59] K. P. Santhosh and V. Bobby Jose, Rom. Rep. Phys. **66**, 939 (2014).

[60] K. P. Santhosh and A. Joseph, Pramana **58**, 611 (2002).
[61] K. P. Santhosh and S. Sabina, Phys. At. Nucl. **75**, 973 (2012).
[62] K. P. Santhosh and V. Bobby Jose, J. Nucl. Phys. Mat. Rad. Appl. **1**, 145 (2014).
[63] J. Blocki, J. Randrup, W. J. Swiatecki, and C. F. Tsang, Ann. Phys. (N.Y.) **105**, 427 (1977).
[64] C. Y. Wong, Phys. Rev. Lett. **31**, 766 (1973).
[65] T. D. Thomas, Phys. Rev. **116**, 703 (1959).
[66] J. Huizenga and G. Igo, Nucl. Phys. **29**, 462 (1961).
[67] J. O. Rasmussen and K. Sugawara-Tanabe, Nucl. Phys. A **171**, 497 (1971).
[68] D. L. Hill and J. A. Wheeler, Phys. Rev. **89**, 1102 (1953).
[69] J. Galin, D. Guerreau, M. Lefort, and X. Tarrago, Phys. Rev. C **9**, 1018 (1974).
[70] H. H. Gutbrod, W. G. Winn, and M. Blann, Nucl. Phys. A **213**, 267 (1973).
[71] D Glas and U. Mosel, Phys. Rev. C **10**, 2620 (1974).
[72] C. C. Sahm, H. G. Clerc, K. H. Schmidt, W. Reisdorf, P. Armbruster, F. P. Heßberger, J. G. Keller, G. Münzenberg, and D. Vermeulen, Nucl. Phys. A **441**, 316 (1985).
[73] P. Armbruster, Rep. Prog. Phys. **62**, 465 (1999).
[74] G. G. Adamian, N. V. Antonenko, and W. Scheid, Nucl. Phys. A **678**, 24 (2000).
[75] V. Zagrebaev, A. Karpov, M. Aritomo, Y. Naumenko, and W. Greiner, Phys. Part. Nucl. **38**, 469 (2007).
[76] J. Błocki, L. Shvedov, and J. Wilczyński, Int. J. Mod. Phys. E **15**, 426 (2006).
[77] K. Siwek-Wilczyańska, A. Borowiec, I. Skwira-Chalot, and J. Wilczyński, Int. J. Mod. Phys. E **17**, 12 (2008).
[78] R. S. Naik, W. Loveland, P. H. Sprunger, A. M. Vinodkumar, D. Peterson, C. L. Jiang, S. Zhu, X. Tang, E. F. Moore, and P. Chowdhury, Phys. Rev. C **76**, 054604 (2007).
[79] Z. H. Liu and J. D. Bao, Phys. Rev. C **81**, 044606 (2010).
[80] R. Yanez, W. Loveland, J. S. Barrett, L. Yao, B. B. Back, S. Zhu, and T. L. Khoo, Phys. Rev. C **88**, 014606 (2013).
[81] R. du Rietz, E. Williams, D. J. Hinde, M. Dasgupta, M. Evers, C. J. Lin, D. H. Luong, C. Simenel, and A. Wakhle, Phys. Rev. C **88**, 054618 (2013).
[82] E. M. Kozulin, G. N. Knyazheva, I. M. Itkis, M. G. Itkis, A. A. Bogachev, E. V. Chernysheva, and L. Krupa, Phys. Rev. C **90**, 054608 (2014).
[83] J. D. Jackson, Can. J. Phys. **34**, 767 (1956).
[84] R. Vandenbosch and J. R. Huizenga, *Nuclear Fission* (Academic, New York, 1973), p. 233.
[85] J. Khuyagbaatar *et al.*, GSI Scientific reports, 2012, p.131.
[86] S. Hofmann, S. Heinz, R. Mann, J. Maurer, G. Münzenberg, S. Antalic, W. Barth, H. G. Burkhard, L. Dahl, K. Eberhardt, R. Grzywacz, J. H. Hamilton, R. A. Henderson, J. M. Kenneally, B. Kindler, I. Kojouharov, R. Lang, B. Lommel, K. Miernik, D. Miller, K. J. Moody, K. Morita, K. Nishio, A. G. Popeko, J. B. Roberto, J. Runke, K. P. Rykaczewski, S. Saro, C. Scheidenberger, H. J. Schött, D. A. Shaughnessy, M. A. Stoyer, P. Thörle-Pospiech, K. Tinschert, N. Trautmann, J. Uusitalo, and A. V. Yeremin, Eur. Phys. J. A **52**, 180 (2016).